

AMERICAN UNIVERSITY OF BEIRUT

SET7 INFLUENCES THE EXPRESSION OF GENES
IMPLICATED IN DIABETIC ENDOTHELIAL
DYSFUNCTION

by
MIRIAM GHASSAN EL BARHOUN

A thesis
submitted in partial fulfillment of the requirements
for the degree of Master of Science
to the Department of Anatomy, Cell Biology and Physiological Sciences
of the Faculty of Medicine
at the American University of Beirut

Beirut, Lebanon
September 2021

AMERICAN UNIVERSITY OF BEIRUT

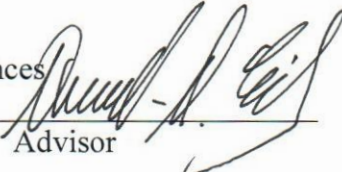
**SET7 INFLUENCES THE EXPRESSION OF GENES
IMPLICATED IN DIABETIC ENDOTHELIAL
DYSFUNCTION**

by


MIRIAM GHASSAN EL BARHOUN

Approved by:


Assaad Eid, DSc, Professor
Department of Anatomy, Cell Biology and Physiological Sciences


Advisor


Abdo Jurjus, PhD, Professor
Department of Anatomy, Cell Biology and Physiological Sciences


Co-Advisor


Rihab Nasr, PhD, Associate Professor
Department of Anatomy, Cell Biology and Physiological Sciences


Member of Committee

Natalie Khoueiry-Zgheib, MD, Professor
Department of Pharmacology and Toxicology


Member of Committee

Assam El-Osta, PhD, Professor
Department of Diabetes, Monash University


Member of Committee

Date of thesis defense: September 13, 2021

AMERICAN UNIVERSITY OF BEIRUT

THESIS RELEASE FORM

Student Name: El Barhoun Miriam Ghassan
Last First Middle

I authorize the American University of Beirut, to: (a) reproduce hard or electronic copies of my thesis; (b) include such copies in the archives and digital repositories of the University; and (c) make freely available such copies to third parties for research or educational purposes:

- As of the date of submission
- One year from the date of submission of my project.
- Two years from the date of submission of my project.
- Three years from the date of submission of my project.



17/09/2021

Signature

Date

ACKNOWLEDGEMENTS

Firstly, I would like to express my deepest gratitude to my main supervisors Dr. Assam El-Osta and Dr. Assaad Eid for their continuous support and guidance throughout my studies. I sincerely thank Dr. Assam El-Osta for welcoming me into the Epigenetics in Human Health and Disease Laboratory and providing me with the opportunity to work in a supportive and nurturing environment. I will cherish the knowledge and experience I have gained during this project.

I would like to thank Dr. Scott Maxwell for his patience and supervision throughout the entirety of this project, his critique and advice were profoundly helpful and fundamental to the completion of this project. You have greatly contributed to my understanding of bioinformatics. I would also like to sincerely thank Dr. Ishant Khurana for taking the time to review and provide constructive criticism during the proof-reading of this thesis.

I am indebted to Dr. Harikrishnan Kaipananickal and Dr. Jun Okabe for sharing their technical expertise and for providing invaluable guidance throughout training and implementing experimental protocols.

You have all contributed to creating an enjoyable and productive work environment that has made this experience truly memorable. Completing this project would not have been possible without the moral and academic support you all provided, for this I am grateful.

ABSTRACT OF THE THESIS OF

Miriam Ghassan El Barhoun

for

Master of Science

Major: Physiology

Title: Set7 Influences the Expression of Genes Implicated in Diabetic Endothelial Dysfunction

The Set7 lysine methyltransferase catalyses mono-methylation of the histone H3 on lysine residue 4 (H3K4me1) and has previously been shown to regulate gene expression. The role of Set7 in diabetic endothelial dysfunction remains poorly understood.

In this study, we examine the influence of Set7 on the expression of genes implicated in diabetes. RNA expression was assessed using a Set7 knock-out animal model and a specific pharmacological inhibitor of the enzyme. Gene set enrichment analysis of RNA sequencing data showed changes in pro-inflammatory gene expression in diabetic complications. To extend our in vivo findings, we examined the pharmacological inhibition of Set7 in cultured human microvascular endothelial cells (HMEC-1) using (R)-PFI-2 and TNF α . Set7-dependent gene expression was analysed by chromatin immunoprecipitation (ChIP) to determine H3K4me1 at gene targets associated with diabetic endothelial dysfunction.

In response to Set7 inhibition, RNA-seq analysis indicated significant differential expression of genes previously shown to be implicated in endothelial dysfunction. We show that H3K4me1 patterns on the selected gene VCAM1 were reduced using the Set7 inhibitor, (R)-PFI-2, which is consistent with its gene suppression. Assessment of multiple genomic regions along VCAM1 revealed a possibly critical region, upstream of the promoter, which was influenced by (R)-PFI-2. In conclusion, Set7 is an epigenetic regulator that is involved in diabetic pathways, as characterized by its regulation of genes implicated in endothelial dysfunction. While further validation of these findings is required, we consider that targeting Set7 may have therapeutic potential in management of diabetes and its complications.

PREFACE

The work presented in this thesis was completed in Epigenetics in Human Health and Disease Laboratory, the Department of Diabetes, Central Clinical School, Monash University. The following experiments were either fully performed or assisted with by individuals other than the candidate.

1. Dr. Jun Okabe of Epigenetics in Human Health and Disease Laboratory, the Department of Diabetes, Central Clinical School, Monash University was involved in:
 - a. Assistance in routine cell culture involving TNF α stimulation of human microvascular endothelial cells (HMEC-1) and Set7 inhibition using (R)-PFI-2.
 - b. Designing primers for specific genes and genomic regions to be used for RT-qPCR and chromatin immunoprecipitation (ChIP) experiments
2. Dr. Harikrishnan Kaipananickal of Epigenetics in Human Health and Disease Laboratory, the Department of Diabetes, Central Clinical School, Monash University was involved in:
 - a. Assisting with RNA extraction from human microvascular endothelial cells
 - b. Assisting with the chromatin immunoprecipitation assay protocol
3. Dr. Scott Maxwell of Epigenetics in Human Health and Disease Laboratory, the Department of Diabetes, Central Clinical School, Monash University was involved in:
 - a. Assisting with and performing multiple Western blots and protein quantification analyses.
 - b. Assisting with and providing guidance with performing complementary cDNA synthesis and RT-qPCR run setup
 - c. Assisting with and performing analysis of computed experimental data (RNA-seq data and RT-qPCR data) using the bioinformatics platforms: RStudio and Partek Flow
4. Dr. Hannah Rodriguez and Dr. Sameer A Jadaan Al-Sarray of Epigenetics in Human Health and Disease Laboratory, the Department of Diabetes, Central Clinical School, Monash University were involved in performing preliminary experiments of generated RNA-seq data sets of the bulk diabetic mouse kidney and TNF α -stimulated HMEC-1 cells treated with the Set7 inhibitor, (R)-PFI-2. These data sets were analysed in this study.

TABLE OF CONTENTS

ACKNOWLEDGEMENTS	1
ABSTRACT.....	2
PREFACE	3
ILLUSTRATIONS.....	8
TABLES.....	10
ABBREVIATIONS	11
LITERATURE REVIEW.....	13
1.1. Diabetes and Its Pathophysiological Manifestations	13
1.2. Endothelial Dysfunction in Diabetes	14
1.3. Epigenetics.....	15
1.4. Chromatin Structure.....	16
1.5. Histone Post-translational Modifications and Regulation of Gene Expression 16	
1.6. Lysine Methylation of Histone Proteins	18
1.7. Histone Methyltransferases and Demethyltransferases	19
1.8. Set7 Lysine Methyltransferase and H3K4 Monomethylation	20
1.9. Set7 and Diabetes-Induced Inflammation.....	21
1.10. Set7 Inhibition.....	22

1.10.1.	(R)-PFI-2.....	23
1.11.	Aims of This Study	23
MATERIALS		25
2.1.	Cell Lines	25
2.2.	Pharmacological Drug Stimulants	25
2.3.	Cell Culture Reagents	25
2.4.	Antibodies	25
2.5.	General Reagents	26
2.6.	Consumables	27
2.7.	Kits.....	27
2.8.	Western Blot Buffers	28
2.9.	Instruments and Equipment	28
2.10.	ChIP Buffers	29
2.11.	Primers	29
2.11.1.	Human cDNA primers	29
2.11.2.	Human ChIP primers	30
METHODS		31
3.1.	Tissue Culture Methods	31
3.1.1.	Cell culture.....	31
3.1.2.	Passaging and splitting cells	31
3.1.3.	Harvesting cells.....	32
3.1.4.	Cell stimulants	32

3.1.4.1.	Pharmacological inhibition with TNF α -induced inflammatory response	32
3.1.4.2.	Determination of optimal (R)-PFI-2 concentration to treat HMEC-1 cells	33
3.1.4.3.	Pharmacological inhibition of Set7 reduces its ubiquitous activity in HMEC-1 cells	33
3.2.	Nucleic Acids Isolation.....	36
3.2.1.	RNA extraction	36
3.2.2.	Complementary DNA synthesis	37
3.2.3.	Measurement of DNA using Qubit Fluorometer	37
3.3.	Chromatin Immunoprecipitation Assay.....	37
3.3.1.	Formaldehyde fixation of cultured cells	37
3.3.2.	Sonication	38
3.3.3.	Reverse crosslinking	39
3.3.4.	DNA column purification	39
3.3.5.	Assessment of chromatin sonication efficiency using MultiNA	40
3.3.6.	Immunoprecipitation.....	40
3.4.	Real-Time Quantitative Polymerase Chain Reaction	42
3.4.1.	Primer design	42
3.4.1.1.	cDNA primers.....	42
3.4.1.2.	ChIP primers	42
3.4.3.	cDNA analysis	43
3.4.4.	ChIP analysis	43
3.4.5.	Statistical analysis of RT-qPCR data.....	43
3.5.	Protein Expression Analysis	44
3.5.1.	Whole cell protein extract.....	44
3.5.2.	Determination of protein concentration using Bradford's assay	44

3.5.3. Immunoblotting	44
3.6. Bioinformatics Methodology	45
3.6.1. Analysis of RNA-Seq Data using Partek Flow.....	45
RESULTS	47
4.1. Overview of experimental study design	47
4.2. Comparison of experimental groups in RNA-seq dataset of diabetic mouse kidney reveals patterns of differential gene regulation.....	49
4.3. Pathway analysis of RNA-Seq data of Set7KO in the diabetic mouse kidney identifies significant genes associated with endothelial dysfunction	52
4.4. HMEC-1 and diabetic mouse kidney show similar changes in endothelial-specific genes associated with inflammatory response.....	55
4.5. Pharmacological inhibition of Set7 in HMEC-1 cells attenuates gene expression changes induced by TNF α	58
4.6. Set7 inhibition alters patterns of H3K4me1 enrichment at several loci across VCAM1	64
DISCUSSION	69
CONCLUSION	83
REFERENCES.....	85

ILLUSTRATIONS

Figure

Set7 inhibition of non-histone modification RPL29me2 using (R)-PFI-2 in HMEC-1 cells.....	35
Comprehensive overview of experimental study design and illustration of experimental approaches implemented throughout the study.....	48
Genome-wide changes in gene expression in different comparative groups induced by Set7KO, ApoE KO and administration of STZ in mouse models	50
Patterns of gene dysregulation in the absence of Set7 between experimental groups to demonstrate the role of Set7 in regulating gene expression profiles in the STZ mouse models	51
Comprehensive overview of computational analysis of diabetic mouse kidney bulk RNA-seq data.....	54
Gene expression patterns of endothelial cell-specific genes dysregulated in HMEC-1 cells	57
Set7 inhibition attenuates gene expression of inflammatory mediators	60
Gene expression profiles implicated in the extracellular matrix regulation	61
Gene expression profiles associated with vascular oxidative stress	62
Gene expression profiles associated with lipid metabolism and cholesterol regulation	63
Comprehensive overview of H3K4me1 enrichment along VCAM1.....	66

H3K4me1 enrichment levels of genomic regions along VCAM1 computed from
RT-qPCR data to investigate association between Set7 inhibition and gene
regulation 67

TABLES

Table

1. Cell line and growth medium constituents used in this study..... 31
2. Experimental conditions of HMEC-1 cell culture used in this study 33

ABBREVIATIONS

Abbreviation	Full
cDNA	Complementary DNA
ChIP	Chromatin immunoprecipitation
DM	Diabetes mellitus
DNA	Deoxyribonucleic acid
ECM	Extracellular matrix
ENCODE	The Encyclopaedia of DNA elements
ET-1	Endothelin
FDR	False discovery rate
GSA	Gene specific analysis
GSEA	Gene set enrichment analysis
H3K4me1	Monomethylation of lysine 4 of histone 3
HKMT	Histone lysine methyltransferase
HMEC-1	Human microvascular endothelial cells
I ₂	Prostaglandin
IGT	Impaired glucose tolerance
LogFC	Log2 of the fold change
LSD1	Lysine-specific demethylase 1
MMP9	Matrix metalloproteinase 9
mRNA	Messenger ribonucleic acid
NF- κ B	Nuclear factor kappa B
NO	Nitric oxide
NOS3	Nitric oxide synthase 3
PRMT	Protein arginine methyltransferases

Abbreviation	Full
PTM	Posttranslational modification
qRT-PCR	Quantitative polymerase chain reaction
RNA	Ribonucleic acid
RNA-seq	RNA-sequencing
ROS	Reactive oxygen species
siRNA	Small interfering RNA
SOD2	Superoxide dismutase 2
STZ	Streptozotocin
T2DM	Type 2 diabetes mellitus
TF	Transcription factor
TGF β	Transforming growth factor beta
TIMP3	Tissue inhibitor of metalloproteinase 3
TNF α	Tumour necrosis factor alpha
TSS	Transcription start site
VCAM1	Vascular cell adhesion molecule 1

CHAPTER 1

LITERATURE REVIEW

1.1. Diabetes and Its Pathophysiological Manifestations

Type 2 diabetes mellitus (DM) is becoming an increasingly common diagnosis among the global population. Chronic hyperglycaemia is the characteristic feature that defines this metabolic disorder. The main driving factor of the progression of type 2 diabetes is metabolic stress, namely prolonged elevation of plasma glucose levels. The aetiology of this disorder includes environmental contributors such as: improper dietary nutrition, physical inactivity, and genetic factors that comprise the interactions within the genome of the individual. Presence of metabolic derangements, induced by obesity and sedentariness, initiate the pathophysiological cascade leading to the development of this disease (Y. Zheng, Ley, & Hu, 2018). The key pathological defects are insulin resistance and impaired insulin secretion. Alterations to environmental risk factors result in elevated glucose levels thus resulting in excessive secretion of insulin to keep up with the demand, ultimately leading to insulin resistance and ineffective action. Compensation by β -cells causes them to further increase insulin and result in hyperinsulinemia. Eventually this leads to the intermediary metabolic state: impaired glucose tolerance (IGT). The cascade continues to reach β -cell dysfunction and failure, causing impaired insulin secretion and hyperglycaemic conditions (Galicia-Garcia et al., 2020). This shifted metabolic state renders the body incapable of maintaining glucose homeostasis, thus ultimately resulting in damage to various organ systems. Diabetic complications can be allocated into two prominent categories: microvascular

(retinopathy, neuropathy, and nephropathy) and macrovascular (cardiovascular disease) complications (Beckman & Creager, 2016).

1.2. Endothelial Dysfunction in Diabetes

The vascular endothelium is comprised of a single layer of endothelial cells that function as a structural barrier between the lumen and surrounding vessel wall. Its basal functions include modulation of vascular homeostasis, regulation of vascular tone through secretion of various growth factors and cytokines, platelet adhesion and aggregation, and regulation of vascular permeability (Heo, Berk, & Abe, 2016). To maintain vascular homeostasis, the endothelium secretes various regulatory mediators and molecules such as extracellular matrix components, nitric oxide (NO), prostaglandin (I₂), endothelin-1 (ET-1), angiotensin II (ANGII), tumour necrosis factor (TNF), and adhesion molecules (e.g. VCAM1, ICAM1) (van den Oever, Raterman, Nurmohamed, & Simsek, 2010). Blood flow is regulated by specific mediators that modulate vascular tone, with the primary vasodilator being nitric oxide (NO) (Poher & Sessa, 2007). The endothelium also plays a role in adaptation to certain stimuli such as oxidative, mechanical, and metabolic stress. Imbalances in these regulatory roles lead to endothelial dysfunction, and ultimately to the genesis of various vascular complications and diseases, such as atherosclerosis (Forstermann, Xia, & Li, 2017; Godo & Shimokawa, 2017). Endothelial dysfunction is characterized by a vasoconstrictive, pro-inflammatory, pro-thrombotic, and oxidant-rich milieu (Sena, Pereira, & Seica, 2013). Manifestations of the dysfunctional state of the endothelium include decreased nitric oxide bioavailability, increased leukocyte migration and adhesion, increased production of reactive oxygen species (ROS), and increased pro-inflammatory signalling (Takeda

et al., 2020). In diabetic conditions, endothelial dysfunction is augmented by metabolic disturbances, such as hyperglycaemia and insulin resistance thus promoting the progression of vascular diseases (Takeda et al., 2020). These all contribute the onset and progression of diabetic vascular complications. Of clinical significance, endothelial dysfunction has been shown to be a possible prognostic approach to predicting future cardiovascular events (Kolluru, Bir, & Kevil, 2012; Takeda et al., 2020). From a clinical perspective, developing therapeutic strategies that target endothelial dysfunction may provide a promising approach to reducing diabetes-associated cardiovascular morbidity and mortality.

1.3. Epigenetics

Despite this disorder being extensively studied, scientists are yet to reach a comprehensive understanding of the underlying mechanisms. Genetic risk factors have been identified through genome-wide association studies (GWAS), which have been able to distinguish certain genes that indicate involvement in the pathogenesis of T2DM. However, in the past recent years, focus has begun to shift towards the epigenome to further clarify GWAS findings (Rosen et al., 2018). The term “epigenetics” has been defined as the modulation of genotypic expression thereby reflecting a corresponding phenotype. In other words, it focuses on the changes in gene expression, triggered by epigenetic modifications, without altering the DNA nucleotide sequence (Dupont, Armant, & Brenner, 2009). These modifying mechanisms include: (1) DNA methylation, (2) histone modifications, and (3) ncRNAs gene regulation. Epigenetic alterations modulate gene expression, where these alterations may either promote gene transcription or repress it (Choudhuri, Cui, & Klaassen, 2010).

1.4. Chromatin Structure

Eukaryotic DNA is packaged into an instructive nuclear structure: chromatin. Chromatin is composed of DNA and associated DNA-binding proteins, forming the scaffold for DNA that can respond to cellular environmental prompts; thereby governing gene regulation and the various ways DNA is utilized. Proteins associated with packaging of DNA into chromatin can be categorized into two principal groups: histone and non-histone proteins. The histone proteins H2A, H2B, H3, and H4 comprise the core of the nucleosome octamer which is constituted of two molecules of each histone and 147 base pairs of two super-helical turns of DNA. An additional histone protein is H1 and acts as a linker between adjacent nucleosomal cores (Fyodorov, Zhou, Skoultchi, & Bai, 2018). Non-histone proteins include those that are involved in RNA transcription, such as polymerases and transcription factors, structural proteins, and histone-like proteins.

1.5. Histone Post-translational Modifications and Regulation of Gene Expression

Genomic expression of sequences is profoundly reliant on transcriptional regulation. Transcription is the process that initiates the cascade to ultimately result in specific gene expression respective to the transcribed DNA sequence. Chromatin accessibility is the primary determinant of transcriptional regulation, whereby it either permits or suppresses accessibility of transcriptional machinery and transcription factors (TFs) to the underlying DNA sequence (Keating & El-Osta, 2013). Chromatin exists in bidirectional alternating structural states: heterochromatin and euchromatin. Euchromatin can be described as a loosened state of chromatin by which it advocates transcriptional activation, whereas heterochromatin is a highly condensed conformation

thereby restricting accessibility to transcriptional machinery (Bannister & Kouzarides, 2011). The conformational state of chromatin is primarily governed by posttranslational modifications (PTMs) that include methylation, acetylation, phosphorylation to either the DNA, histones, or both. Posttranslational modifications (PTMs) have been shown to be profoundly influential upon regulation of gene transcription and therefore cell identity. PTMs include transient histone modifications that involve acetylation, glutathionylation, methylation, phosphorylation, sumoylation, and ubiquitination (Choudhuri et al., 2010; Strahl & Allis, 2000).

Histone modifications play a central role in the regulation of transcriptional machinery and chromatin structure, subsequently altering gene expression. Key epigenetic players that are responsible for adding, removing, and recognizing these PTMs have been referred to as writers, erasers, and readers respectively. ‘Writers’ are enzymes that catalyse the addition of histone PTMs, ‘erasers’ are enzymes that remove chemical tags on modified histones, and ‘readers’ are distinct effector proteins that identify and interpret histone PTMs to mediate downstream signalling (Chan & Maze, 2020; Hyun, Jeon, Park, & Kim, 2017). Thus, histone PTMs exert their effects in two distinctive ways, either by directly influencing the conformational structure of chromatin or by regulation of the binding of effector molecules. Conversely, new studies have demonstrated that nonenzymatic mechanisms, such as interaction of histones with small, reactive molecules, for example metabolites and toxins, could induce histone PTMs. Therefore, this negates the notion that histone modifications require writers, readers, and erasers to be of biological significance (Chan & Maze, 2020; Q. Zheng, Prescott, Maksimovic, & David, 2019). The ability of modified core histone proteins to regulate transcriptional gene expression has been demonstrated in

several studies, with extensive emphasis on phosphorylation, methylation, and acetylation (Hornbeck et al., 2012).

1.6. Lysine Methylation of Histone Proteins

Histone lysine methylation was first reported with the discovery of the histone lysine methyltransferase (HKMT), Su(var)3-9 homologue 1 (SUV39H1), that specifically methylates H3K9 (Rea et al., 2000). Since then, various methyltransferases, demethyltransferases, and their respective inhibitors have been identified. Histone lysine methylation occurs on the amino N-terminal of histones, where one or more methyl groups are added to lysine residues. Lysines may be mono-, di-, or tri-methylated, which adds a degree of complexity to the understanding of this modification and its functional responses. In contrast to histone acetylation, which is associated with transcriptional activation, histone methylation can either result in gene activation or repression. For example, transcriptional activation is characteristic of lysine methylation at H3K4, H3K36, and H3K79. On the other hand, methylated lysine residues of H3K9, H3K27, and H4K20, are associated with transcriptional repression (Sims, Nishioka, & Reinberg, 2003). The bidirectionality of the outcome of lysine methylation is dependent on the specificity of the modified residue and the number of covalently bonded methyl groups (Bannister & Kouzarides, 2011; Y. Zhang & Reinberg, 2001). The versatility of lysine methylation may be an outcome of the site-specificity of histone methylation; methyl groups may be transferred to histone tails, linker histones, or globular domains (Bannister & Kouzarides, 2011). Additionally, the degree of methylation on a lysine residue may result in various functional outcomes pertaining to transcriptional regulation. Monomethylation of H3K27 has been shown to

be associated with transcriptional activation, whereas tri-methylation of this same residue indicates transcriptional repression (Barski et al., 2007; Ferrari et al., 2014). Histone methylation of specific lysine residues appears to have a prominent influence on transcriptional outcomes and assigning further biological significance is under extensive study.

1.7. Histone Methyltransferases and Demethyltransferases

Histone lysine methyltransferases (HKMTs) are the enzymes that catalyse the methylation of lysine residues of histones. HKMTs mediate the transfer of a methyl group from S-adenosylmethionine (SAM), a cofactor for lysine methylation reactions, to the N-terminal of a lysine residue (Yu & Zhuang, 2019). HKMTs are further divided into two families based on their catalytic domain: SET-domain containing HKMTs, which includes Su(var)3-9, Enhancer of zeste(E(z)), and trithorax, and non-SET-domain containing HKMTs, such as Dot1L (Dillon, Zhang, Trievel, & Cheng, 2005; Jenuwein, 2006). HKMTs are relatively specific enzymes that modify specific lysines in varying degrees. To illustrate, H3K9 is specifically tri-methylated by *Neurospora crassa* DIM5 whereas H3K4 is mono-methylated by SET7/9 (Tamaru et al., 2003; Xiao et al., 2003). Histone methylation was initially thought to be an irreversible modification that was involved in modulation of genome expression (Kouzarides, 2002), however the discovery of histone demethyltransferases refuted this notion and revealed that lysine methylation is dynamically regulated. Identification of the first histone lysine demethyltransferase, lysine-specific demethylase 1 (LSD1), which is an amine oxidase that demethylates H3K4, provided evidence that histone methylation is enzymatically reversible (Shi et al., 2004). This discovery revealed an underlying mechanism for

transient histone methylation marks and subsequent mediation of gene expression. It is important to note that these enzymes also exhibit substrate and site specificity; some enzymes are only able to demethylate mono- and demethylated lysine residues, while other enzymes are capable of demethylating all states of methylated lysines (Bannister & Kouzarides, 2011). For example, LSD1 is only capable of demethylating mono- or demethylated H3 lysine 4, and not tri-methylated lysine 4 (Shi et al., 2004). Transient histone modifications and their respective enzymes remain under investigation, as not all have been discovered.

1.8. Set7 Lysine Methyltransferase and H3K4 Monomethylation

H3K4 methylation is a histone modification commonly associated with transcriptional activation and it is prominently enriched at enhancer regions, promoter regions and transcription start sites (TSS) (Hyun et al., 2017; Noma, Allis, & Grewal, 2001). Transcriptional gene regulation is dependent on the position of methylated lysine residues and the degree of methylation and is a hallmark of specific chromosomal structures and nuclear processes. (Hyun et al., 2017; Santos-Rosa et al., 2002). The three methylated states of lysine 4 on H3, H3K4me1, H3K4me2, and H3K4me3, have been shown to be differentially distributed along proximal and distal regulatory regions. H3K4me1 is predominantly localized at enhancer regions, H3K4me2 and H3K4me3 are enriched at 5' end of actively transcribing genes, and H3K4me3 enrichment has been shown at promoter regions (Heintzman et al., 2007; Hyun et al., 2017; Santos-Rosa et al., 2002).

Set7 (also referred to as Set7/9, Set9, or KMT7), is a lysine SET-domain methyltransferase that catalyses the monomethylation of H3K4. The 41 kilo Dalton

(kDa) protein was originally identified in HeLa cells and extensive analysis of its structural components have revealed its functional contribution to H3K4 monomethylation (H3K4me1) (Veerappan, Avramova, & Moriyama, 2008; Wilson et al., 2002). Additionally, chromatin immunoprecipitation (ChIP) experiments have reported the role of Set7 in H3K4me1 enrichment at enhancer and promoter regions of certain genes (Brasacchio et al., 2009; El-Osta et al., 2008). Conversely, several studies have demonstrated that the histone H3 is not the sole primary substrate of Set7. For instance, a previous study reported that Set7-deficient mouse embryonic fibroblasts exhibited no fluctuations in H3K4 methylation levels (Lehnertz et al., 2011). This led to the postulation that Set7 also potentially mediates the lysine methylation of certain non-histone substrates and numerous substrates have been subsequently identified: Rpl29, p53, DNMT1, sex hormone receptors, and NF- κ B (Chuikov et al., 2004; Esteve et al., 2009; Hamidi et al., 2018; Subramanian et al., 2008; X. Zhang, Huang, & Shi, 2015).

1.9. Set7 and Diabetes-Induced Inflammation

Several studies have demonstrated the association between Set7 activity and inflammatory events in hyperglycaemic conditions. Monomethylation of H3K4 by Set7 regulates expression profiles of genes involved in inflammation (Brasacchio et al., 2009). In diabetic mouse models, macrophages showed increased Set7 recruitment and inflammatory gene expression. Loss of function studies using siRNA exhibited reduced TNF α -induced recruitment of NF- κ B subunit p65 to inflammatory gene promoters (Li et al., 2008; Yu & Zhuang, 2019). Another study has also demonstrated the Set7-mediated transcriptional activation of inflammatory genes, such as NF- κ B subunit p65,

in transient hyperglycaemic conditions (El-Osta et al., 2008). Pertaining to the role of Set7 in vascular endothelial dysfunction, it has also been demonstrated that Set7 may activate the transcription of inflammatory genes via H3K4me1-independent mechanisms in hyperglycaemic conditions (Okabe et al., 2012). These findings collectively suggest the involvement of Set7 in regulation of inflammatory events within a diabetic milieu. The use of selective pharmacological inhibitors could provide a platform to target and modulate persistent inflammatory events and reduce the risk of further macrovascular complications.

1.10. Set7 Inhibition

Development of a pharmacological therapeutic approach targeting the enzymes responsible for post-translational modifications is on the rise. Set7 has been shown to be of clinical significance in hyperglycaemic settings and targeting this methyltransferase is a potential approach to reducing pathological complications (El-Osta et al., 2008; Okabe et al., 2012). Several Set7 inhibitors, specific and non-specific, have been proposed and have demonstrated inhibition of the HKMT. Non-specific inhibitors that are capable of inhibiting Set7 include specific protein arginine methyltransferases (PRMTs) inhibitors, such as arginine methyltransferase inhibitor (AMI) compounds. A study using the compounds AMI-1 and AMI-5 investigated the impact on Set7 activity in endothelial cells (Okabe et al., 2014). Additionally, a study utilized a selective HKMT inhibitor, sinefungin, an antifungal agent, to investigate epigenetic changes in the human kidney mediated by Set7 (Sasaki et al., 2016). Recently discovered Set7 inhibitors, (R)-PFI-2 and cyproheptadine hydrochloride (CYP), have been shown to specifically inhibit Set7 and are potential candidates for therapeutic use through

modulation of transcriptional changes mediated by Set7 (Barysyt-Lovejoy et al., 2014; Takemoto et al., 2016).

1.10.1. (R)-PFI-2

High-throughput screening and optimisation of a library generated from an in vitro methylation assay resulted in the synthesis of the first selective Set7 inhibitor, (R)-PFI-2. Comparison of the structural binding to Set7 between the enantiomers of the compound, (S)-PFI-2 and (R)-PFI-2, illustrated that (R)-PFI-2 inhibited human Set7 by 500-fold whereas (S)-PFI-2 was rendered the inactive form of the drug. The use of (R)-PFI-2 to provide further insight into the regulatory roles of Set7 in disease settings could prove to be useful as a platform for the use of selective inhibitors as therapeutic agents.

1.11. Aims of This Study

The main aim of this study is to evaluate the gene expression changes in response to Set7 inhibition using (R)-PFI-2 in human microvascular endothelial cells. Additionally, we aim to assess the interaction between (R)-PFI-2 and Set7 on differentially expressed genes implicated in TNF α -induced inflammation and examine changes in histone methylation patterns. Attenuation of gene changes induced by inflammation at a transcriptional level may enable the use of epigenetic inhibitors to be used in a clinical setting.

The specific aims of this study are as follow:

1. To analyse gene expression data from experimental models of Set7 inhibition using (R)-PFI-2
2. To evaluate the effect of Set7 inhibition on the regulation of the endothelial transcriptome in diabetic vascular inflammatory conditions
3. To investigate and identify the potentiality of Set7 inhibition using (R)-PFI-2 to attenuate TNF α -mediated inflammation in human microvascular endothelial cells (HMEC-1)

CHAPTER 2

MATERIALS

2.1. Cell Lines

Cell lines	Supplier
Human microvascular endothelial cells (CRL-3243)	American Type Culture Collection (ATTC)

2.2. Pharmacological Drug Stimulants

Reagent	Supplier
PFI	Cayman Chemical
Human Recombinant TNF α (#300-01A)	Peprotech

2.3. Cell Culture Reagents

Reagent	Supplier
0.5% Trypsin-EDTA (10x)	Gibco
Antibiotic-Antimycotic (100X), liquid	Gibco
Dimethylsulfoxide (DMSO)	Sigma-Aldrich
Fetal bovine serum (FBS)	Bovogen
GlutaMAX (100X)	Gibco
MCDB 131 medium	Gibco
Phosphate buffered saline (PBS)	Gibco

2.4. Antibodies

Antibody	Supplier
Donkey Anti-Mouse secondary antibody (800nm)	Li-Cor
Goat Anti-Rabbit secondary antibody (680nm)	Li-Cor
H3K4me1 (8895)	Abcam
RPL29 (88514)	Abcam
RPL29me2 (D8T9P)	Cell Signalling Technology

2.5. General Reagents

Reagent	Supplier
10X RT Random Primer	Applied Biosystems
Albumin standard (2mg/ml)	Thermo Scientific
Bradford reagent	Sigma Life Science
BSA standard (23209)	Thermo Scientific
Chloroform	Sigma-Aldrich
Dithithreitol (DTT)	GE Health
DNA Wash Buffer	Zymo Research
dNTP mix (100mM)	Applied Biosystems
Dynabeads Protein A	Invitrogen
EDTA (Ethylenediaminetetraacetic acid)	Sigma-Aldrich
Ethanol (100%)	Sigma-Aldrich
Formaldehyde 37%	Sigma-Aldrich
Glycerol	Amresco
Glycine	Sigma-Aldrich
Hepes-KOH (pH 7.9)	Amresco
Magnesium chloride (MgCl ₂)	Sigma-Aldrich
NaCl	Sigma-Aldrich
NP-40	Fluka
Nuclease-free H ₂ O	Zymo-Research
Phenylmethylsulfonyl (PMSF)	Sigma-Aldrich
Potassium chloride (KOH)	Fluka
Precision ® FAST 2X qPCR Master Mix with LR and SY	Primer Design
Proteinase inhibitor cocktail	Takara
Proteinase inhibitor	Sigma-Aldrich
Proteinase K	Sigma-Aldrich
Quant-iT 1X dsDNA HS Working Solution	Invitrogen
Qubit dsDNA HS Standard #1	Invitrogen
Reverse Transcriptase	Invitrogen
Reverse Transcriptase Buffer	Applied Biosystems
Sodium dodecyl sulphate (SDS)	Bio-Rad
Tris Base	Formedium
Tris-EDTA (TE) buffer	Sigma-Aldrich
TRIZOL® Reagent (15596-026)	Invitrogen
Tween-20	Sigma-Aldrich

2.6. Consumables

Equipment	Supplier
1.5 ml microtubes	Sarstedt
100mm x 20mm cell culture dishes	Corning
10mL stripette	Costar
15 mL centrifuge tube	Corning
150cm ² cell culture flask	Corning
1cc/mL syringe	Terumo
2 ml microtubes	Sarstedt
21G needle	Terumo
25mL stripette	Costar
2mL stripette	Costar
50 mL self-standing centrifuge tube	Corning
5mL stripette	Costar
75cm ² cell culture flask	Corning
96-well Microtest Plate	Sarstedt
Cell scraper	Sarstedt
Cell strainer	Falcon
Countess cell counting chamber slide	Invitrogen
Microamp 96-well optical plate	Applied Biosystems
Mini-PROTEAN TGX Precast Gels	Bio-Rad
NucleoSpin Gel and PCR Clean-up Columns (Ref: 740609.250S)	Macherey-Nagel
Trans-Blot Turbo Transfer Packs	Bio-Rad

2.7. Kits

Product	Supplier
Direct-zol RNA MiniPrep	Zymo Research
DNA Extraction (NTI Binding Buffer, NT3 Wash Buffer, and NE Elution Buffer)	Macherey-Nagel
MultiNA DNA-2500 Reagent kit	Shimadzu
MultiNA RNA Reagent kit	Shimadzu

2.8. Western Blot Buffers

Buffer	Constituents/ Supplier
10X Tris/Glycine/SDS Buffer	Bio-Rad
Intercept Blocking Buffer	LI-COR
NuPAGE LDS Sample Buffer	Invitrogen
TBS	1M Tris Base + 5M NaCl
TBST (5X)	1M Tris Base + 5M NaCl + Tween-20
Whole cell protein extract lysis buffer	20mM Hepes-KOH (pH 7.9), 25% Glycerol, 520mM KCl, 5mM MgCl ₂ , 0.1mM EDTA, 1mM DTT, 0.5mM PMSF, 0.2% NP-40, Proteinase inhibitor P8340

2.9. Instruments and Equipment

Equipment	Supplier
AirClean 600 PCR Workstation	AirClean
Allegra X-12R Centrifuge	Beckman Coulter
Biological Safety Cabinet Class II	CCL Pty Ltd
Centrifuge 5427 R	Eppendorf
Centrifuge 5415 D	Eppendorf
CLARIOstar Microplate Reader	BMG LABTECH
CO ₂ Incubator	Thermo Scientific
Countess II	Life Technologies
Mini Trans-Blot Cell	Bio-Rad
MultiNA	Shimadzu
Odyssey CLx	LI-COR
Power-Pac	Bio-Rad
QSonica Sonicator	QSonica
QuantStudio 3 Real-Time PCR System	Applied Biosystems
Qubit 3 Fluorometer	Invitrogen
SimpliAmp Thermal Cycler	Applied Biosystems
Suspension Mixer (Rotator)	Ratek
Thermomixer comfort	Eppendorf
Trans-Blot Turbo Transfer System	Bio-Rad
Vortex Mixer	Ratek

2.10. ChIP Buffers

Buffer	Constituents
ChIP dilution buffer	0.01% SDS, 1.1% Triton X-100, 1.2mM EDTA, 16.7mM Tris-HCl pH 8.0, 167mM NaCl
ChIP elution buffer	1% SDS, 5mM EDTA, 20mM Tris-HCl pH 8.1, 50mM NaCl
High Salt buffer	0.1% SDS, 1% Triton X-100, 2mM EDTA, 20mM Tris-HCl pH 8.1, 500mM NaCl
LiCl buffer	0.25M LiCl, 1% NP-40, 1% deoxycholic acid sodium salt, 1mM EDTA, 10mM Tris-HCl pH 8.1
Low Salt buffer	0.1% SDS, 1% Triton X-100, 2mM EDTA, 20mM Tris-HCl pH 8.1, 150mM NaCl
Sodium dodecyl (lauryl) sulfate (SDS) lysis buffer	1% SDS, 10mM EDTA, 50mM Tris-HCl pH 8.1
TE + 0.01% SDS	10mM Tris pH 8.1, 1mM EDTA, 0.01% SDS
TE buffer	10mM Tris pH 8.1, 1mM EDTA

2.11. Primers

2.11.1. Human cDNA primers

Name	Forward sequence	Reverse sequence
VCAM1	CAAAGGCAGAGTACGCAAACAC	GCTGACCAAGACGGTTGTATCTC
SOD2	TAGGGCTGAGGTTTGTCCAG	GGAGAAGTACCAGGAGGCCGT
MMP9	GCACTGCAGGATGTCATAGG	ACGACGTCTTCCAGTACCGA
NOS3	ATGGAGAGAGCTTTGCAGCTGCC	AGGACACCAGTGGGTCTGAGCA
ANGPTL4	TGCAAGATGACCTCAGATGGAGGC	AGAACTCGCCGTGGGGATCCC
IL1B	TGCACGCTCCGGGACTCACA	CATGGAGAACACCACTTGTGCTCC
CCL2	AGCAAGTGTCCCAAAGAAGC	TGGAATCCTGAACCCACTTC
TIMP3	ACCGAGGCTTCACCAAGATG	CCATCATAGACGCGACCTGT

2.11.2. Human ChIP primers

Name	Forward sequence	Reverse sequence
h_VCAM1_R2_ChIP	GCTATGAGGATGGAAGATTCTGGA	CACTGACAGCACCTTTATCATTCC
h_VCAM1_R3_ChIP	TCATGTCAGCCTCCCAGTTC	TGGATTCTTGGACAAGGGCT
h_VCAM1_R4_ChIP	CTGAGAGTGTCAAAGAAGGAGACA	CTCCCGCATCCTTCAACTGG
h_VCAM1_R5_ChIP	TCAAGCACAGCTGCTTTATCC	CCTCCCGGGAAAAGGTTTGA
h_VCAM1_R6_ChIP	ACACCCCTTGCACACCAATTA	AATAGCCAAGTGCCAGACCTC
h_VCAM1_R7_ChIP	TTGGTTGACCTCCAGTGATTAGA	AGCATCATGTGACCACACAAGTA
h_VCAM1_U3(R1)_ChIP	AAGCCCCATCTGGACATAGTAAG	AATTTGGCATTTCAGGTGGACA
h_VCAM1_U2(R2)_ChIP	GCAAATTGCAAGCAAGCTTTTAG	GCCAACTAGATTCAAAAATTCCCTG
h_VCAM1_D1(R2)_ChIP	GATGTTAAGGAACCACCAGGGAT	GAACTCCTGATTAGAGGAAGTTGGA
VCAM1-H3k4m1 ChIP(R3) P2	ATTTCACTCCGCGGTATCTG	ACCCTTATTTGTGTCCCACCT
VCAM1-H3k4m1 ChIP(R2) P1	GCTTCATTCTGCAATCAGCA	AACCCCTTCAGTTGCTCTCA

CHAPTER 3

METHODS

3.1. Tissue Culture Methods

3.1.1. Cell culture

The cell line used in this study is immortalized human microvascular endothelial cells (HMEC-1). Cells were incubated at 37°C in a 5% CO₂ humidified incubator. The cells were cultured in MCDB 131(1X) media supplemented with Antibiotic-Antimycotic, Glutamax and heat-inactivated foetal bovine serum (FBS). The table below describes the proportion of media supplements used for the cell line.

Cell line	Details	Growth Medium Constituents
HMEC-1 cells	Endothelial, adherent, transformed	MCDB 131(1X), FBS (5% v/v), GLutaMAX (100X), Anti-Anti (100X)

Table 1: Cell line and growth medium constituents used in this study

3.1.2. Passaging and splitting cells

To sub-culture, the cells were washed with PBS and detached from the tissue culture flasks using trypsin-EDTA solution (1-2 ml depending on the flask size). The action of trypsin was deactivated by adding 5X the volume of growth media. The cell suspension solution was transferred to a Falcon conical centrifuge tube (15 ml or 50 ml) and pelleted by centrifugation at ___rpm (300g) for 3 minutes at 4°C. The supernatant was discarded, and the cells were resuspended in 10 ml of growth media. Cells were reseeded at a specific density for either further culture or for *in vitro* experiments. Volume of the cell suspension for reseeded was determined by performing a cell count.

Using a cell counting chamber slide, 10ul of the cell suspension was added to the slide which was then subsequently inserted into the Countess™ II Automated Cell Counter. Based on the estimated cell count, calculations were made to determine the volume required to reseed the desired number of cells. The suspended cells were sub-cultured into corresponding new tissue culture flasks, plates or dishes containing fresh growth media.

3.1.3. Harvesting cells

The growth medium of the adherent cells was aspirated, and cells were subsequently washed with 1 ml of refrigerated PBS (4°C). The first PBS wash was followed by addition of 1 ml of PBS and scraping of the tissue culture dish or plate using a standard cell scraper. Scraped cells were transferred to corresponding 1.5 ml Eppendorf tubes for further analysis through additional *in vitro* experiments.

3.1.4. Cell stimulants

3.1.4.1. Pharmacological inhibition with TNF α -induced inflammatory response

To study gene expression in response to an inflammatory stimulus alongside pharmacological inhibitory treatment, cultured HMEC-1 cells were treated with TNF α and PFI. Cells were seeded at a density of 6×10^6 into 100 mm treated cell culture dishes. Adherent cells were treated for a period of three days with a PFI concentration of 15 μ M, using a dilution factor of $\frac{1}{1000}$. The constituents of each experimental treatment condition are detailed in the table below. TNF α was added using a dilution factor of $\frac{1}{5000}$. Cells were harvested on the fourth day.

	Treatment Condition			
	Control	TNF α	PFI	PFI+TNF α
TNF α	-	2 μ l	-	2 μ l
PFI (15 mM)	-	-	10 μ l	10 μ l
DMSO	10 μ l	-	-	-
Conditional media (1% FBS)	10 ml	10 ml	10 ml	10 ml

Table 2: Experimental conditions of HMEC-1 cell culture used in this study

3.1.4.2. Determination of optimal (R)-PFI-2 concentration to treat HMEC-1 cells

To examine and confirm the effectiveness of the pharmacological inhibitor PFI, HMEC-1 cells were treated at different PFI concentrations to determine the threshold at which inhibition would occur. Cells were seeded in 6-well plates. PFI was prepared in mM at the desired concentrations by dissolving the PFI in DMSO and then performing serial dilutions for the remaining concentrations. The PFI concentrations at which cells were treated are 0 μ M, 0.5 μ M, 1 μ M, 2.5 μ M, 5 μ M, 15 μ M, 25 μ M, 35 μ M. Conditional media (2 ml of 1% v/v heat inactivated FBS, MCDB 131 (1X)) was added to each well with each corresponding PFI treatment (2 μ l PFI (mM)) being added using a $\frac{1}{1000}$ dilution factor. The PFI treatments were prepared and added to the corresponding wells over a period of 3 days. Cells were harvested on the fourth day.

3.1.4.3. Pharmacological inhibition of Set7 reduces its ubiquitous activity in HMEC-1 cells

Dose-curve experiments were carried out to establish a relationship between inhibition of Set7-mediated histone modifications and the molar concentration of (R)-

PFI-2. Major methylation substrates of Set7 include histone H3 lysine residue 4 and the non-histone substrate RPL29, an integral ribosomal protein of the 60S ribosomal subunit (Hamidi et al., 2018). The molecular activity of Set7 is evident upon detection of the presence of methylated substrates that include monomethylated histone H3K4me1 and di-methylated RPL29me2. Based on this information, immunoblotting along with subsequent protein quantification, were completed to validate the association of the substrate RPL29 with Set7, thus allowing us to determine an optimal effective concentration of (R)-PFI-2 to use in treatment conditions and ensure appropriate inhibition of Set7. The ratio of RPL29me2 relative to total RPL29 with respect to PFI (μM) was used to examine the extent of Set7 inhibition (Figure 1). As (R)-PFI-2 concentration increases, a gradual decrease in methylated RPL29me2 is observed, thus indicating successful inhibition of Set7. The optimal concentration of (R)-PFI-2 appears to range from $15\mu\text{M}$ to $25\mu\text{M}$, however $15\mu\text{M}$ (R)-PFI-2 was used in subsequent experiments since the possible risk of (R)-PFI-2-induced cytotoxicity increases at higher concentrations. The steep decrease at $35\mu\text{M}$ in comparison to the gradual decrements of the other molar concentrations serves as an indication of possible cell death occurring at this specific concentration. Cell proliferation and viability could have possibly been compromised at this high concentration.

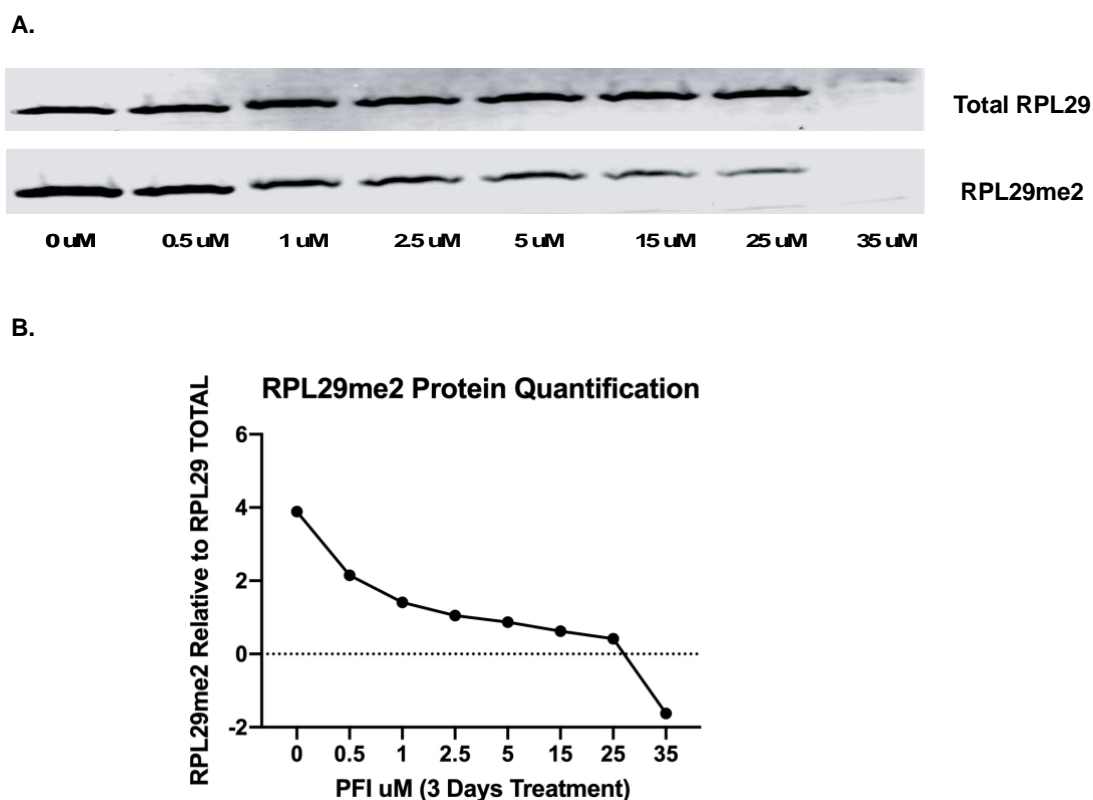


Figure 1: Set7 inhibition of non-histone modification RPL29me2 using (R)-PFI-2 in HMEC-1 cells

HMEC-1 cells were treated with increasing incremental concentrations of PFI (μM) over the course of a 3-day (72 hours) treatment period. The subsequent whole cell protein extraction lysate was immunoblotted with the appropriate antibodies and further analysed and quantified by Odyssey. **A.** Protein extracts from HMEC-1 cells were immunoblotted with antibodies to RPL29 (loading control) and RPL29me2. **B.** Graph illustrating the quantitative analysis of the immunoblotted proteins whereby a ratio was established between the total RPL29 and dimethylated RPL29me2 to illustrate the gradual inhibition of Set7 by (R)-PFI-2 with increasing concentration of this pharmacological inhibitory agent.

3.2. Nucleic Acids Isolation

3.2.1. RNA extraction

Adherent cells were washed twice with ice cold PBS and subsequently scraped and transferred to 2 ml Eppendorf tubes. 500µl of TRIzol was added followed by incubation of the samples on a rotating wheel for 15 minutes at room temperature. 100 µl of chloroform (1:5 ratio) was then added to each sample and vortexed for 30 seconds. Samples were then centrifuged for 15 minutes at 14000 rpm at 4°C. The clear supernatant (upper aqueous phase), which contains the RNA, was collected into a new tube. Equal volume of 100% ethanol was added to the collected supernatant to precipitate the RNA and thoroughly mixed. The isopropanol mixture was then transferred to Zymo-spin IIC column tubes and centrifuged for 30 seconds at 12000 rpm followed by removal of waste fraction. 400 µl of RNA wash buffer was added, and samples were centrifuged again for 30 seconds at 12000 rpm and flowthrough was discarded. DNase solution (5 µl DNase and 75 µl DNA digestion buffer) was prepared and added to the samples which were then left to incubate at room temperature for 15 minutes. 400 µl of Direct-zol RNA Prewash was added to the column tubes and centrifuged for 30 seconds at 12000 rpm. Flowthrough was discarded and 700 µl of RNA wash buffer was added and centrifuged for 30 seconds at 12000 rpm. The waste fraction was removed, and samples were centrifuged again for 3 minutes at 12000 rpm. Column tubes were transferred to new 1.5ml Eppendorf tubes and left to dry for 5 minutes at room temperature. RNA was eluted with 35µl of nuclease free-water and incubated for 1 minute at room temperature followed by centrifugation for 1 minute at 12000 rpm. RNA quantification and assessment of its quality was completed using MultiNA.

3.2.2. Complementary DNA synthesis

The reverse transcription master mix was prepared and is constituted of 2 μ l of Reverse Transcriptase buffer, 2 μ l of random primer, 1 μ l of deoxyribonucleic triphosphate (dNTP), 1 μ l of reverse transcriptase. For each sample, 1 μ g of RNA was added to the master mix alongside the addition nuclease-free water to result in a total reaction volume of 20 μ l for each RNA sample. The cDNA synthesis reaction was then executed in a thermal cycler by firstly incubating the samples at 37°C for 2 hours and then 85°C for 5 minutes. The cDNA samples were then diluted to 80 μ l with RNase-free water and either directly used for qPCR or stored at -20°C.

3.2.3. Measurement of DNA using Qubit Fluorometer

Quantification of DNA was performed by the Qubit Fluorometer and the corresponding Quant-iT reagents using the Qubit dsDNA High Sensitivity assay. Two standards were prepared in 0.5 ml tubes where 190 μ l of Qubit working solution was added to 10 μ l of each Qubit standard (provided in the kit). To quantify the DNA samples, 200 μ l of working solution was added to 1 μ l of each sample and vortexed briefly. Samples were then run on the Qubit Fluorometer and the computed concentrations were collected.

3.3. Chromatin Immunoprecipitation Assay

3.3.1. Formaldehyde fixation of cultured cells

Adherent cells were washed twice with ice-cold PBS and were scraped using a standard cell scraper and transferred to 2ml Eppendorf tubes. Cells were centrifuged at

5000 rpm for 2 minutes and subsequently washed twice with ice-cold PBS. Fixation of the cells consisted of adding 27 μ l of 37 % formaldehyde (final concentration 1% formaldehyde) in 1 ml of fresh PBS and were left to incubate for 6 minutes on rotating wheel at room temperature. After incubation, cells were centrifuged at 5000 rpm for 2 minutes and were subsequently washed again with ice-cold PBS. Cells were centrifuged once more at 5000 rpm for 2 minutes and the PBS wash was aspirated. The formaldehyde reaction was quenched with 0.125M glycine in fresh PBS and the tubes were placed on a rotating wheel to incubate for 6 minutes at room temperature. The fixed cells were centrifuged at 1200 rpm for 3 minutes at 4°C to obtain a pellet. The cells were washed twice with PBS. The supernatant was disposed of and the pellet was resuspended in 300 μ l of SDS lysis buffer supplemented with protease inhibitor (1X). The fixated cells were either directly sonicated or frozen at -80°C until required use.

3.3.2. Sonication

Sonication was performed using the QSonica sonicator. The fixated lysed cells were sonicated for 10 minutes (high power, interval: 30 seconds on, 30 seconds off) to shear the chromatin to optimal lengths approximately between 200-300 bp. Each lysed sample (300 μ l) was appropriately inserted in the QSonica tube holder apparatus in a chilled water bath 4°C. After completing sonication, the samples were centrifuged at 13000rpm for 5 minutes at 4°C. The supernatant was transferred to a new Eppendorf tube and the pellet of cell debris was disposed of. The effectiveness of the chromatin shearing was assessed by MultiNA. Any samples that required additional shearing were further sonicated for the appropriate duration. Following completion of sonication, chromatin samples were centrifuged at 13000 rpm for 5 minutes and the supernatant

was collected into new Eppendorf tubes for chromatin quantification using the Qubit Fluorometer.

3.3.3. Reverse crosslinking

To assess the effectiveness of sonication, 10µl of the sheared chromatin samples was made up to 100µl with ChIP elution buffer with the addition of 2µl of proteinase K. The chromatin samples were incubated for 2 hours at 62°C on a thermomixer shaking at 1400 rpm to implement reverse crosslinking.

3.3.4. DNA column purification

After completion of reverse crosslinking, DNA column purification was performed using the NucleoSpin extraction kit. The buffers and column tubes were all provided in the kit. NT1 binding buffer (300µl) was added and thoroughly mixed with the eluted samples, which were then transferred to DNA purification column tubes. The column tubes were centrifuged for 30 seconds at 13000 rpm and followed by disposal of the waste fractions. NT3 washing buffer (700µl) was added to the column tubes and centrifuged for 30 seconds at 13000 rpm. The waste fractions were discarded, and the column tubes were centrifuged again for two minutes at 13000 rpm to remove any remaining wash buffer. The column tubes were then transferred to Eppendorf tubes and left open to completely dry for three minutes to ensure there are no remnants of the wash buffer. NE elution buffer (60µl) was added to the column tubes which were left to incubate for one minute prior to centrifugation at 13000rpm for one minute. The Qubit Fluorometer was used to quantify the DNA samples. The eluted DNA samples were then stored at -20°C until further use in subsequent quantitative analysis.

3.3.5. Assessment of chromatin sonication efficiency using MultiNA

Efficiency of chromatin shearing was evaluated using the MultiNA DNA2500 kit on the MultiNA for separation of DNA between 100-2500 bp based on the manufacturer's instructions. 5 μ l of a size marker pGEM DNA ladder was diluted in 1:75 TE buffer. 3 μ l of purified DNA from each sample was used. Computation of the required volumes of DNA 2500 separation buffer, SYBR Gold nucleic gel stain, and DNA 2500 markers were generated by the MultiNA control software. Sonication efficiency was determined based on the optimal size range of 200-350 bp. Any samples that did not fall in this range were re-sonicated.

3.3.6. Immunoprecipitation

Prior to immunoprecipitation, a preclearing step was implemented with the aim of reducing any potential background noise that may interfere with the specific binding of the antibody (Ab). 10 μ l of washed magnetic Dynabeads were added to the sonicated chromatin samples and incubated for an hour at 4°C on a rotating wheel. Samples were then centrifuged at 2000 rpm for 30 seconds followed by collection of the supernatant in new 1.5ml Eppendorf tubes using a magnetic rack.

To prepare each ChIP, 5 μ g of soluble chromatin was used for the Ab and IgG control tubes, whereas 10% of the IgG reaction volume was used for the input control tubes. The volumes of the Ab and IgG samples were made up to 500 μ l by adding ChIP dilution buffer with proteinase inhibitor (1X). Each Ab sample was incubated with 20 μ l of washed magnetic Dynabeads and 3 μ l of the anti-histone H3 monomethyl K4 antibody on a rotating wheel at 4°C overnight for approximately 17 hours. For each sample, a negative control was also prepared, whereby a non-specific antibody (IgG

control) was added to the corresponding samples and incubated overnight with the same components as the Ab samples. An input control was also prepared whereby no antibody was added to the chromatin and set aside until reverse crosslinking.

Following incubation, Ab and IgG tubes were centrifuged at 2500 rpm for 30 seconds and placed on a magnetic rack. The supernatant containing the unbound fraction was discarded and the Dynabeads were washed consecutively with 1 ml of the following refrigerated buffers in this listed sequence: low salt wash buffer, high salt wash buffer, LiCl wash buffer, TE wash buffer, and TE + 0.01% SDS wash buffer. Each wash consisted of placing the samples on a magnetic rack, removing the previous wash buffer, adding the new wash buffer, placing on rotating wheel for three minutes, centrifuging for 30 seconds at 2500 rpm, and once again removing the wash buffer. This sequence of steps was repeated for each wash buffer. After completion of the last wash, the beads of Ab and IgG samples were resuspended with 100 μ l of ChIP elution buffer, which was also added to the input control samples. 2 μ l of proteinase K was added to the bound DNA (Ab and IgG) and input control samples, which were then incubated on a thermomixer at 62°C for two hours with shaking at 1400 rpm to achieve reverse crosslinking. DNA was recovered by DNA column purification (section___). Samples were eluted with 60 μ l of NE elution buffer. Downstream analysis by RT-qPCR was then performed on purified samples.

3.4. Real-Time Quantitative Polymerase Chain Reaction

3.4.1. Primer design

3.4.1.1. cDNA primers

Primers for RT-qPCR were designed using the NCBI Primer Blast software to give a final length between 100-200 bp and have melting temperatures around 60°C. Primers were designed in accordance with UCSC softwares (ENCODE and In-Silico PCR) to ensure that the regions of interest are amplified.

3.4.1.2. ChIP primers

Primers for RT-qPCR were designed using the NCBI Primer Blast software to give a final length between 100-200 bp and have melting temperatures around 60°C. Primers were designed in accordance with UCSC softwares (ENCODE and In-Silico PCR) to ensure that the regions of interest are amplified. Selected regions were those that had H3K4me1 peaks along the span of the VCAM1 gene that would indicate an increase in methylation. The array of designed primers included promotor, exonic, intronic, and possible enhancer regions, where H3K4me1 peaks were present.

3.4.2. RT-qPCR master mix preparation and run setup

Real-time quantitative polymerase chain reaction (RT-qPCR) amplification was performed using the QuantStudio 3 Real-Time PCR System. To prepare the master mix for each sample, 2µl of cDNA or ChIP sample, 6.5 µl of Precision® FAST 2X qPCR Master Mix, 0.25 µl of the forward primer, 0.25 µl of the reverse primer, and 3 µl of nuclease-free water was added into each well of the 96-well plate. Reactions were incubated for 10 minutes at 95°C, followed by 40 cycles of 95°C for 10 seconds and

60°C for 30 seconds per cycle. Results were then analysed using the QuantStudio Design and Analysis Software and relative fold changes were computed using the $2^{-\Delta\Delta Ct}$ method for cDNA samples and the % input method for ChIP samples.

3.4.3. cDNA analysis

Normalization of expression levels was achieved by using H3F3A (H3.3 Histone A) as the housekeeping gene. Using the $2^{-\Delta\Delta Ct}$ method, first ΔCt was computed to determine relative gene expression: $\Delta Ct = Ct (\text{Gene of interest}) - Ct (\text{H3F3A})$. Fold change was then calculated by first calculating $\Delta\Delta Ct = \Delta Ct (\text{Experimental sample}) - \Delta Ct (\text{Control average})$, followed by fold change in gene expression = $2^{-(\Delta\Delta Ct)}$.

3.4.4. ChIP analysis

The method used to normalize the ChIP-qPCR data was the % input method. ChIP-qPCR data was analysed using this method to account for normalization to the amount of input chromatin. The input values were adjusted from 10% to 100% using log base 2 of a dilution factor of 10.

$$\% \text{ Input} = 100 \times 2^{(\text{Adjusted input} - Ct \text{ of specific Ab})}$$

3.4.5. Statistical analysis of RT-qPCR data

Results were plotted and visualized using GraphPad Prism (Version 8.3.1). The mean \pm standard error (SEM) is presented, alongside the computed p-value where $p < 0.05$ is statistically significant. Comparison of the different groups was completed using an ordinary one-way ANOVA test.

3.5. Protein Expression Analysis

3.5.1. Whole cell protein extract

Cultured cells in 6-well plates were washed with ice-cold PBS and scraped with a standard cell scraper. The contents of each well were transferred to 1.5 ml Eppendorf tubes and centrifuged at 8000 rpm for 2 minutes to obtain the pellet. The supernatant was discarded, and the pellet was resuspended with 100 μ l of the whole cell protein extract lysis buffer. The cells were then repeatedly lysed five times with a 21G needle and then left incubate on a rotating wheel at 4°C for 20 minutes. Samples were then centrifuged at 13500 rpm for 15 minutes at 4°C. The supernatants were collected and transferred to new 1.5 ml Eppendorf tubes which were either used directly for further analysis or stored at -20°C until further use.

3.5.2. Determination of protein concentration using Bradford's assay

Protein concentration was measured by the means of the Bradford assay. 250 μ l of Bradford's reagent was added to 5 μ l of each of the BSA standards and 5 μ l of each protein sample in the wells of a 96-well assay plate. Absorbance readings were measured at 595 nm using the Clariostar Microplate Reader. The relative protein concentrations were determined by plotting the standard curve from the absorbance values of the BSA standards.

3.5.3. Immunoblotting

Analysis of the expression of proteins of interest was completed using SDS-PAGE. Whole cell lysates (30 μ g) were combined with NuPAGE LDS sample buffer (4X) and DTT (dithiothreitol) (50mM). Protein samples were then placed on a heating

block at 95°C for 5 minutes to denature the proteins. Samples were then quickly loaded into 4–15% Mini-PROTEAN® TGX™ precast protein gels, alongside the pre-stained molecular weight size standard SeeBlue® Plus2. The gel was run in Bio-Rad Tris/Glycine/SDS Buffer (1X) at 200 V for 30-45 minutes, until the marker dye had reached the end of the gel. The separated proteins were transferred from the gel to a Trans-Blot Turbo Mini 0.2 µm PVDF Transfer membrane using the Trans-Blot® Turbo™ Transfer system for 7 minutes at a constant current of 1.3A (up to 25 V). Following the transfer, the membrane was first washed with TBS (1X) and then blocked for 45 minutes with blocking buffer. The membrane was incubated overnight at 4°C with the primary antibody RPL29me2 (rabbit), diluted in blocking buffer (1:2000 dilution). Following primary antibody incubation, the membrane was washed 4 times for 5 minutes each in TBST(1X) on a rocker at room temperature. Secondary antibody incubation was then performed by adding the secondary antibodies (listed in materials) diluted in TBST (1X) (1:10,000 dilution) for one hour at room temperature. The membrane was washed 4 times for 5 minutes each with TBST (1X). Scanned with LICOR Odyssey.

3.6. Bioinformatics Methodology

3.6.1. Analysis of RNA-Seq Data using Partek Flow

Fastq files from previously performed RNA-sequencing of Set7KO/ ApoE^{-/-} diabetic kidney tissue of mice were imported into the bioinformatics software Partek Flow and sample attributes were assigned accordingly to each group. Following STAR alignment to the mus musculus genome (mm10) and quantification to an annotation model (Partek E/M), the generated reads were filtered (maximum ≤ 10) and the

resultant gene transcripts were normalized by counts per million (CPM) and subjected to differential gene specific analysis (GSA). Differentially regulated genes were determined by applying the filter features $FDR < 0.05$ and $p < 0.05$. Enrichment scores of gene sets were identified using gene set enrichment analysis (GSEA).

CHAPTER 4

RESULTS

4.1. Overview of experimental study design

In order to highlight the role of Set7 inhibition, we adopted an experimental study design to assess the function of Set7 in gene regulation (Figure 2). The foundation of our study was based on the two experimental models, *in vivo* mouse model with genetically inhibited Set7 and *in vitro* HMEC-1 cell culture models with pharmacologically inhibited Set7. RNA-seq data sets of these two experimental models were analysed and specific genes of statistical and biological significance in a diabetic milieu were selected for functional analysis (*VCAM1*, *SOD2*, *NOS3*, *ANGPTL4*, *MMP9*, *TIMP3*, *IL1B*, and *CCL2*). Differential gene expression changes were further validated *in vitro* in HMEC-1 cells, stimulated with TNF α and treated with (R)-PFI-2 to inhibit Set7 using qPCR. In order, to investigate the role of Set7 in regulating gene expression, chromatin immunoprecipitation was performed to detect changes in H3K4me1 enrichment patterns, specifically along regions of the gene *VCAM1*.

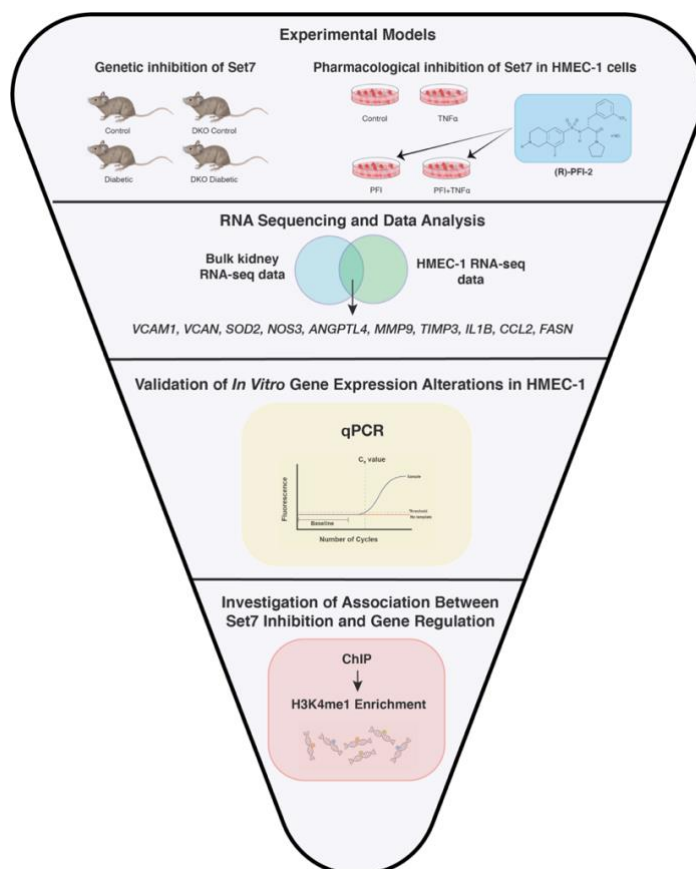


Figure 2: Comprehensive overview of experimental study design and illustration of experimental approaches implemented throughout the study

Experimental models were comprised of diabetic mouse models and HMEC-1 cell culture, where diabetes was induced using streptozotocin (STZ) and $\text{TNF}\alpha$ respectively. *Set7* was inhibited by genetic knockout using a viral vector in the mouse models and by a pharmacological agent (R)-PFI-2 in cell culture. Kidney dissection followed by preparation protocols for RNA sequencing were completed. RNA-seq data analysis revealed several genes of interest that are potential contributors to diabetic complications. Gene expression changes were validated in *Set7* inhibited HMEC-1 cell culture treated with $\text{TNF}\alpha$, using qPCR. H3K4me1 enrichment patterns were investigated across *VCAM1* gene to assess the possible association between *Set7* activity and gene regulation.

4.2. Comparison of experimental groups in RNA-seq dataset of diabetic mouse kidney reveals patterns of differential gene regulation

Using the RNA-seq data set of the diabetic mouse kidney, differential gene expression changes are shown in volcano plots (Figure 3. and 4.) to provide an overview of differential gene activity between experimental groups. RNA-sequencing detected a total of 19263 genes.

Comparative analysis of the Diabetic vs. Control group showed that 7483 genes were statistically significant ($p \leq 0.05$), after the exclusion of the fold change (FC) range -2 to 2, 887 genes were upregulated, and 316 genes were downregulated. The DKO Diabetic vs. Diabetic group had 215 upregulated genes, and 160 downregulated genes ($p \leq 0.05$; FC range -2 to 2). The DKO Control vs. Control group 156 upregulated genes, and 170 downregulated genes ($p \leq 0.05$; FC range -2 to 2). The DKO Diabetic vs. DKO Control group 533 upregulated genes, and 42 downregulated genes ($p \leq 0.05$; FC range -2 to 2). Taken together, these differential gene expression changes are indicative of the effects of diabetic conditions and Set7 inhibition, which were selected for further analysis to establish biological significance.

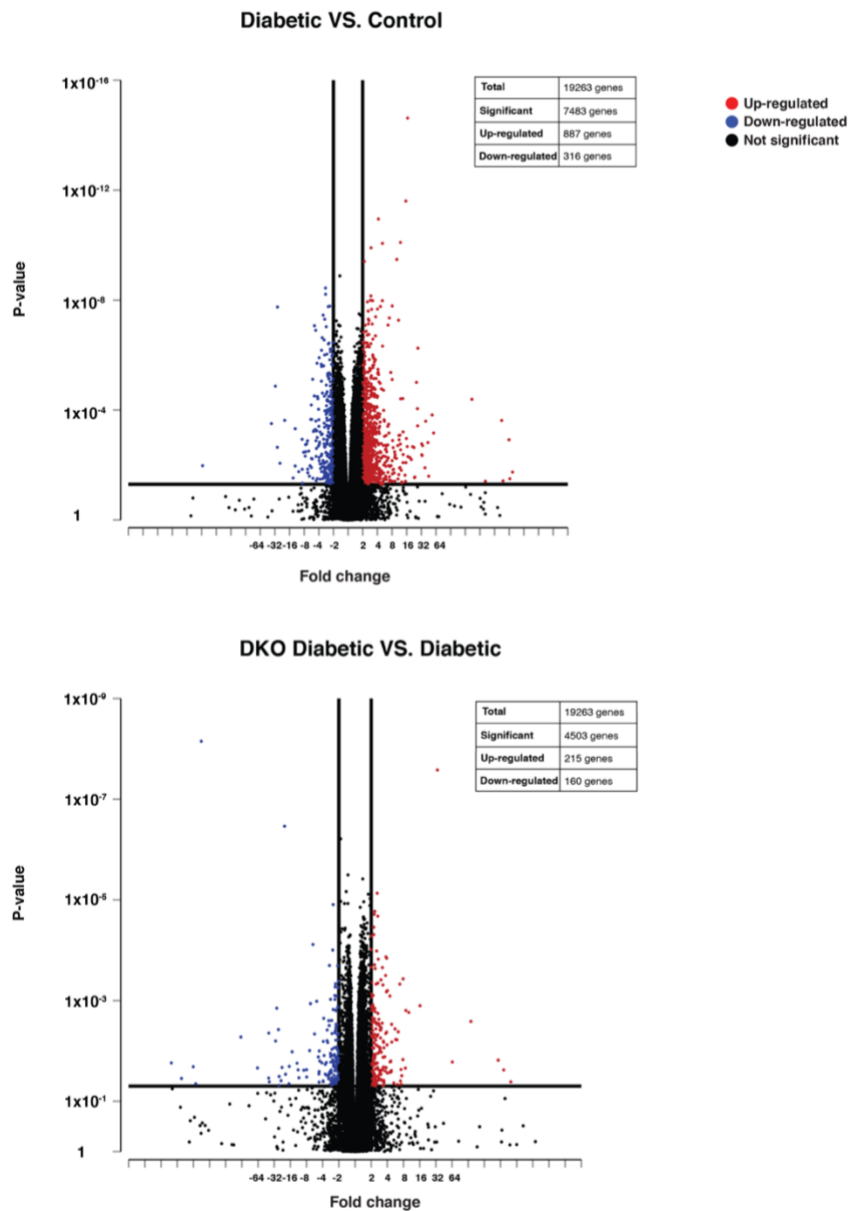


Figure 3: Genome-wide changes in gene expression in different comparative groups induced by Set7KO, ApoE KO and administration of STZ in mouse models

Volcano plots were generated in Partek Flow®. Significantly upregulated genes are shown in red and downregulated genes are shown in blue ($p \leq 0.05$). The fold change (FC) range of -2 to 2 was excluded when filtering for significant differentially regulated genes.

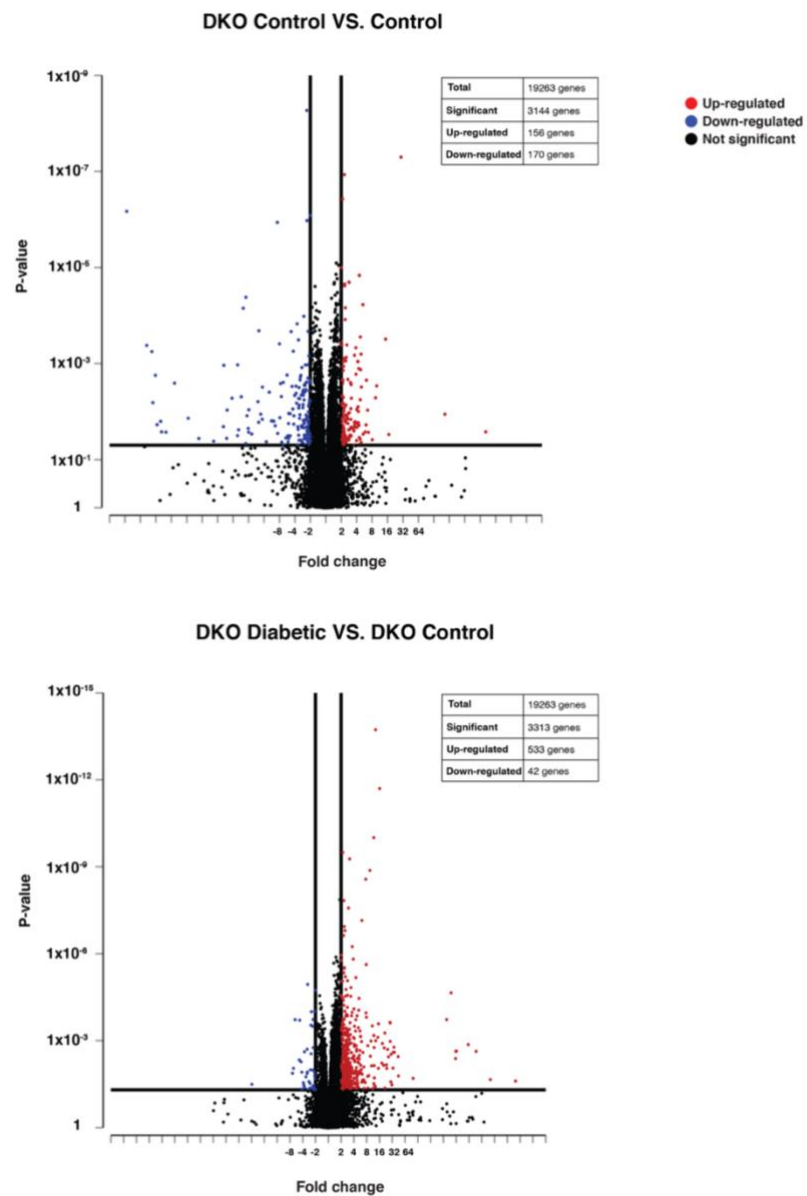


Figure 4: Patterns of gene dysregulation in the absence of Set7 between experimental groups to demonstrate the role of Set7 in regulating gene expression profiles in the STZ mouse models

Volcano plots were generated in Partek Flow®. Significantly upregulated genes are shown in red and downregulated genes are shown in blue ($p \leq 0.05$). The fold change range (FC) of -2 to 2 was excluded when filtering for significant differentially regulated genes.

4.3. Pathway analysis of RNA-Seq data of Set7KO in the diabetic mouse kidney identifies significant genes associated with endothelial dysfunction

Previous studies have shown strong association of Set7 in gene regulation, specifically in genes related to endothelial dysfunction in diabetes (Brasacchio et al., 2009; Paneni et al., 2015). As an initial approach to exemplify the functionality of Set7 and its subsequent inhibition within diabetic endothelial dysfunction, we analysed previously sequenced bulk RNA-Seq data of Set7-knockout (-/-) and ApoE-knockout (-/-) diabetic mouse kidney using the software Partek Flow®. Genome-wide changes in gene expression induced by Set7KO were analysed by GSEA to assign biological functional significance to the data set. Briefly, using GSEA the gene expression data from diabetic mouse kidney was intersected with a publicly available gene set repository, Gene Ontology (GO), downloaded from the Molecular Signature Database (MSigDB) (<https://www.gsea-msigdb.org/gsea/msigdb>). GSEA analysis identified gene sets grouped based on their association with specific biological processes. Enrichment scores (ES) are allocated to each gene set, reflecting the extent of overrepresentation or underrepresentation of genes in a pathway.

A comprehensive figure was generated in RStudio to visualize the enrichment score patterns of gene sets and the corresponding genes of interest in the experimental conditions (Figure 5). Generated differential pathway results were based on the contrasts between the experimental conditions, diabetic vs. control and double-knockout diabetic (DKO) vs. diabetic (Figure 5A). Gene sets were ranked based on false discovery rate ($FDR \leq 0.05$). The log fold changes of differentially regulated genes were plotted within their corresponding gene sets and were ranked by statistical significance ($FDR \leq 0.05$) (Figure 5.C).

Computational analysis using GSEA was indicative of genome-wide changes imposed by the knockout of *Set7* in the diabetic mouse kidney tissue based on the DKO Diabetic vs. Diabetic comparison, to highlight the activity of *Set7* and its effects on gene expression. Most importantly, we show pathways that are reversed by *Set7* genetic inhibition (Diabetic vs. Control and DKO Diabetic vs. Diabetic). Top pathways that were upregulated in diabetic conditions and reversed in *Set7* KO include cytokine activity, carboxylic acid binding, inflammatory response, oxidoreductase activity, regulation of peptidase activity, and negative regulation of hydrolase activity. Pathways that were downregulated in diabetic mouse kidney and subsequently upregulated in *Set7* KO include cell regulatory processes such as cellular response to growth factor stimulus, regulation of mRNA metabolic process, transcription regulatory region DNA binding, and cell projection assembly.

From these significant dysregulated pathways associated with diabetic endothelial function, several genes including *VCAM1*, *SOD2*, *NOS3*, *ANGPTL4*, *MMP9*, *TIMP3*, *IL1B*, and *CCL2*, were assessed in human microvascular endothelial cells (HMEC-1).

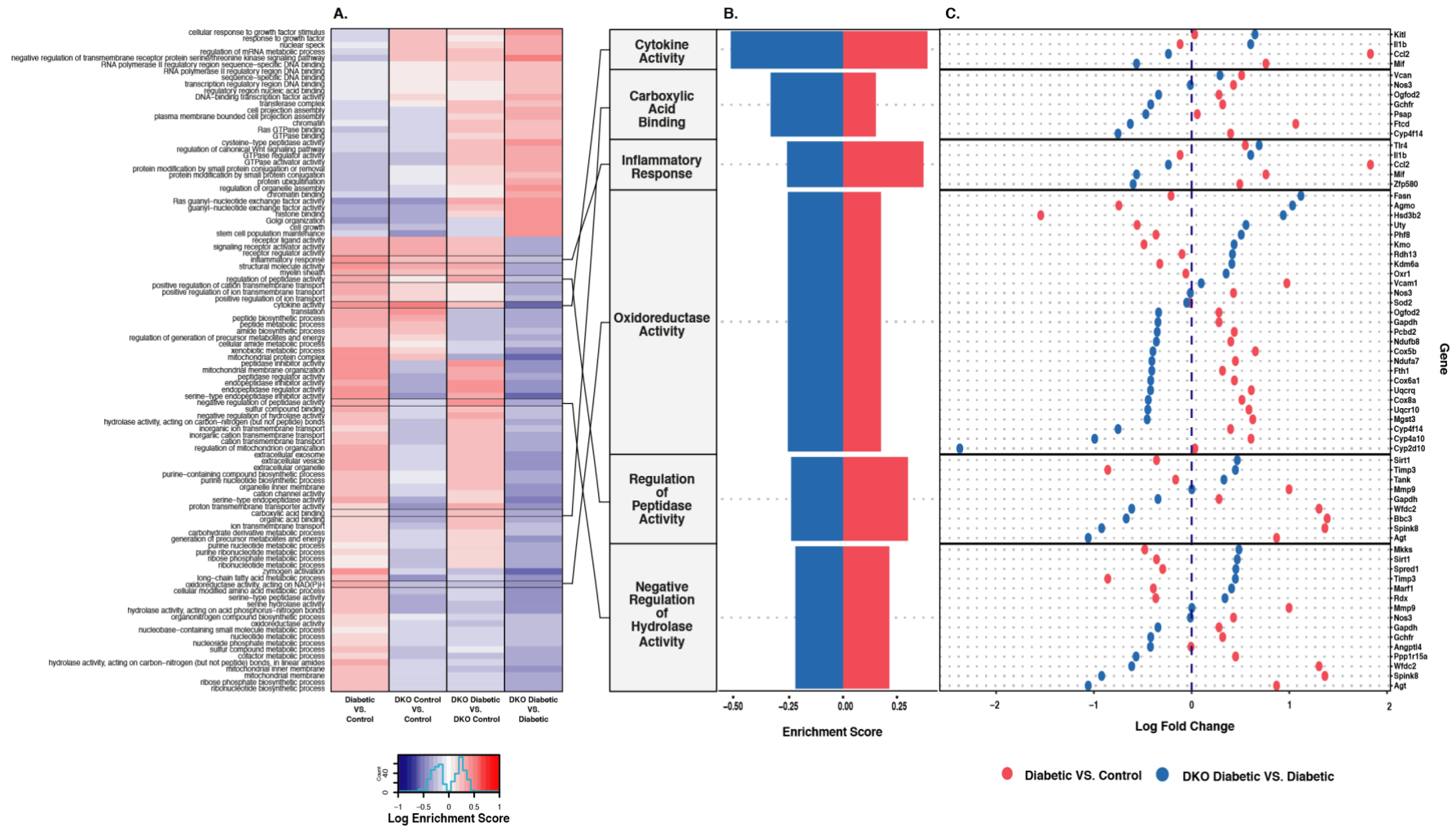


Figure 5: Comprehensive overview of computational analysis of diabetic mouse kidney bulk RNA-seq data

Figure 5: Comprehensive overview of computational analysis of diabetic mouse kidney bulk RNA-seq data

A. Colour-coded heat map of upregulated (white to red) and downregulated (white to blue) gene sets based on filtering by statistical significance of $p \leq 0.05$ and $FDR \leq 0.05$ in the comparison groups Diabetic vs. Control and DKO Diabetic vs. Diabetic. **B.** The graph depicts the enrichment scores of the selected gene sets branching from the heat map. Positive values indicate upregulation and negative values indicate downregulation of gene sets **C.** The log fold change of differentially regulated genes within the selected gene sets are plotted. Opposing directions (positive and negative) indicate reversal of gene expression changes between the comparison groups. These genes were empirically selected based on statistical parameters used for selection criteria include $p \leq 0.05$ and $FDR \leq 0.05$.

4.4. HMEC-1 and diabetic mouse kidney show similar changes in endothelial-specific genes associated with inflammatory response

Following the pathway analysis of the bulk RNA-seq of diabetic mouse kidney, we analysed HMEC-1 RNA-seq for an endothelial cell-specific approach to examine the correlation between the gene expression patterns of the two data sets.

The experimental groups that were compared include $TNF\alpha$ vs. Control and PFI+ $TNF\alpha$ vs. $TNF\alpha$ and expression are plotted (Figure 6). Comparison of the fold changes (Log₂ scale) of the selected genes reveal that gene expression patterns are similar in diabetic mouse and human endothelial cells.

In HMEC-1 cells treated with $TNF\alpha$ vs Control group, *VCAM1*, *CCL2*, *IL1B*, *MMP9*, and *SOD2* were upregulated; from this *VCAM1*, *CCL2*, and *MMP9* showed

similar patterns of gene with the bulk RNA-seq of diabetic mouse kidney. *NOS3* was downregulated in the TNF α vs Control group, however it was upregulated in the diabetic mouse kidney. *TIMP3*, a key regulator of ECM showed no activity in HMEC-1 cells, however, it was significantly downregulated in the diabetic mouse kidney.

Next, we show gene expression changes caused by Set7 inhibition in the groups DKO Diabetic vs. Diabetic and PFI+ TNF α vs. TNF α shows that *CCL2* was downregulated and *IL1B* was upregulated by Set7 inhibition in both genetic and pharmacological models. Interestingly, *VCAM1*, *MMP9*, *TIMP3*, *NOS3*, *SOD2* gene expression profiles were inversely correlated between the two data sets.

Overall, differential gene expression patterns are similar between the two data sets and this provides a foundation to investigate the functionality of Set7 and its role in gene regulation within the scope of diabetic endothelial dysfunction.

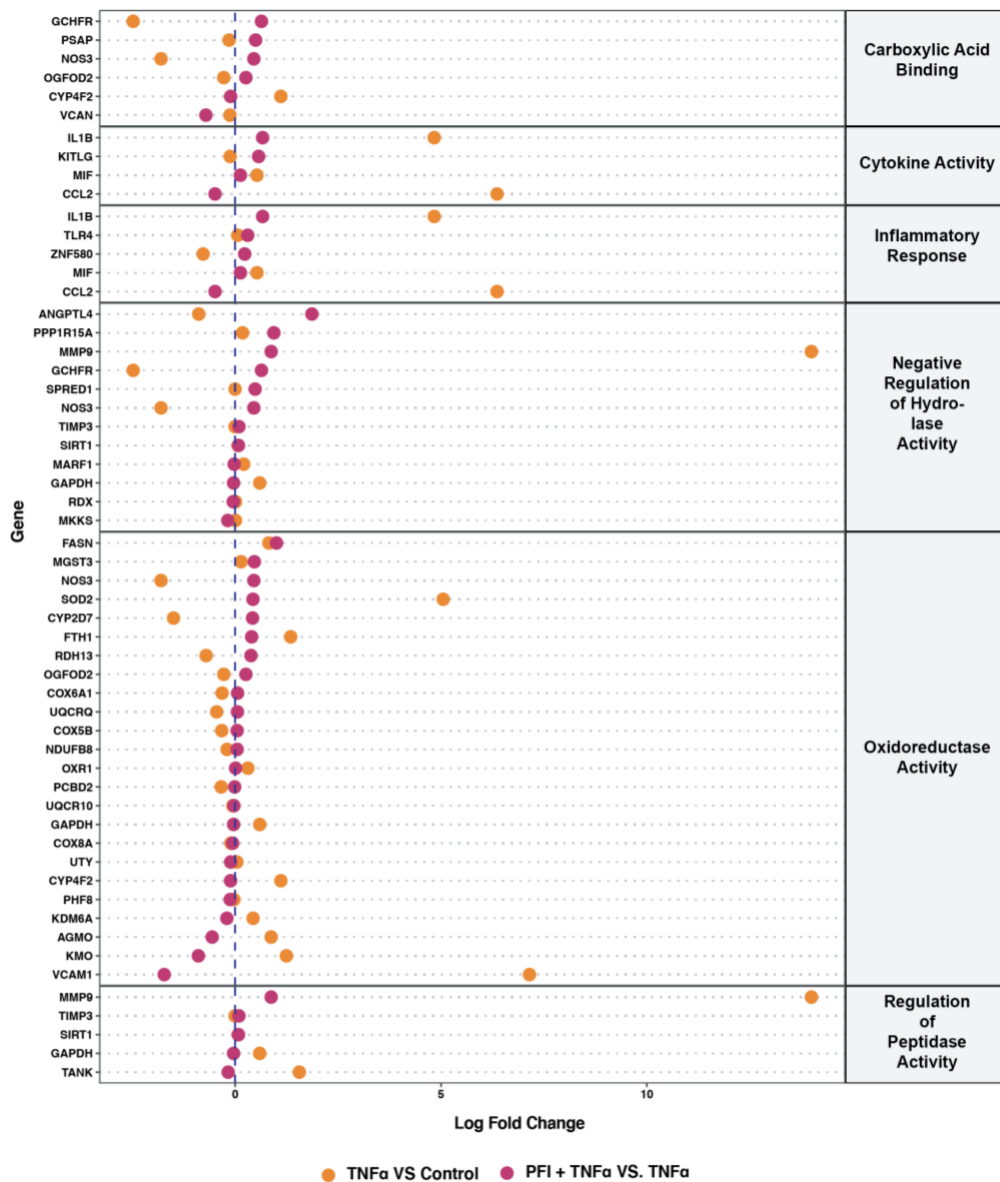


Figure 6: Gene expression patterns of endothelial cell-specific genes dysregulated in HMEC-1 cells

Plot shows fold changes (Log₂ scale) of endothelial cell-specific genes identified from diabetic mouse kidney in endothelial cells exposed to TNF α . Data shows changes in gene expression of HMEC-1 cells exposed to TNF α compared to control (orange) and (R)-PFI-2 + TNF α compared to TNF α (magenta).

4.5. Pharmacological inhibition of Set7 in HMEC-1 cells attenuates gene expression changes induced by TNF α

One of the primary causal contributors to diabetic endothelial dysfunction is induction of inflammation characterized by the upregulation of inflammatory markers, cytokines, and chemokines (Steyers & Miller, 2014). TNF α is a recognized potent stimulator of inflammation in various tissues and organs. To simulate diabetic inflammatory conditions, HMEC-1 cells were exposed to TNF α and the Set7 inhibitor PFI and gene expression profiles of *VCAM1*, *SOD2*, *MMP9*, *NOS3*, *ANGPTL4*, *IL1B*, *CCL2*, and *TIMP3* were evaluated by qPCR in the following experimental groups: TNF α , PFI, and PFI+TNF α . We show significant upregulation of *VCAM1*, *SOD2*, *MMP9*, *NOS3*, *IL1B*, *CCL2*, and *TIMP3*, whereas *ANGPTL4* was downregulated in response to TNF α compared the controls (Figure 7-10).

TNF α upregulated genes implicated in immune response signalling (Figure 7C). *VCAM1*, *IL1B*, and *CCL2* were significantly upregulated in response to TNF α (**** p < 0.0001). Gene expression profiles were consistent for inflammatory mediators upregulated in diabetic conditions (Figure 7A and 7B). Next, we examined if (R)-PFI-2 could reverse changes in gene expression induced by TNF α . Interestingly, (R)-PFI-2 initiated changes in the endothelial transcriptome in normal conditions (PFI vs. Control) and reversed the expression of inflammatory genes induced by TNF α (PFI + TNF α . vs. TNF α .). The results observed in HMEC-1 cells are consistent the gene expression profiles obtained from the RNA-seq data sets (Figure 7A-C).

Extracellular matrix regulation and oxidative stress mechanisms are also altered in diabetic conditions; thus, we show the expression profiles of *NOS3*, *SOD2*, *TIMP3*, and *MMP9* (Figure 8A and Figure 9A).

Regulators of the extracellular matrix, *TIMP3* and *MMP9*, showed increased gene expression in the TNF α stimulated HMEC-1 RNA-seq, however (R)-PFI-2 did not attenuate *TIMP3* and *MMP9* expression. Conversely, validation in the *in vitro models* showed reduction in *TIMP3* and *MMP9* expression in response to (R)-PFI-2 in diabetic inflammatory conditions (Figure 8B and 8C).

Genes implicated in vascular oxidative stress, *NOS3* and *SOD2*, were upregulated in response to TNF α . Addition of PFI to TNF α resulted in further upregulation of gene expression relative to the TNF α group (Figure 9B and 9C).

Genes that are associated with lipid metabolism and cholesterol biosynthesis were also further assessed. *ANGPTL4* exhibited decreased expression in response to TNF α (Figure 10B and 10C); these findings are not consistent with the bulk kidney RNA-seq results (Figure 10A). Set7 inhibition using (R)-PFI-2 in the presence of TNF α notably reversed *ANGPTL4* expression in HMEC-1 cells (Figure 10C).

Taken together, expression profiles of genes associated with inflammation, ECM regulation, vascular oxidative stress, and lipid metabolism (Figures 7-10) were validated in RT-qPCR and showed similar signatures for several genes compared to the RNA-seq. Further analyses would be required to gain an understanding of the transcriptomic regulation of these individual genes, but for this study, we were primarily interested in inflammatory markers, specifically *VCAM1*.

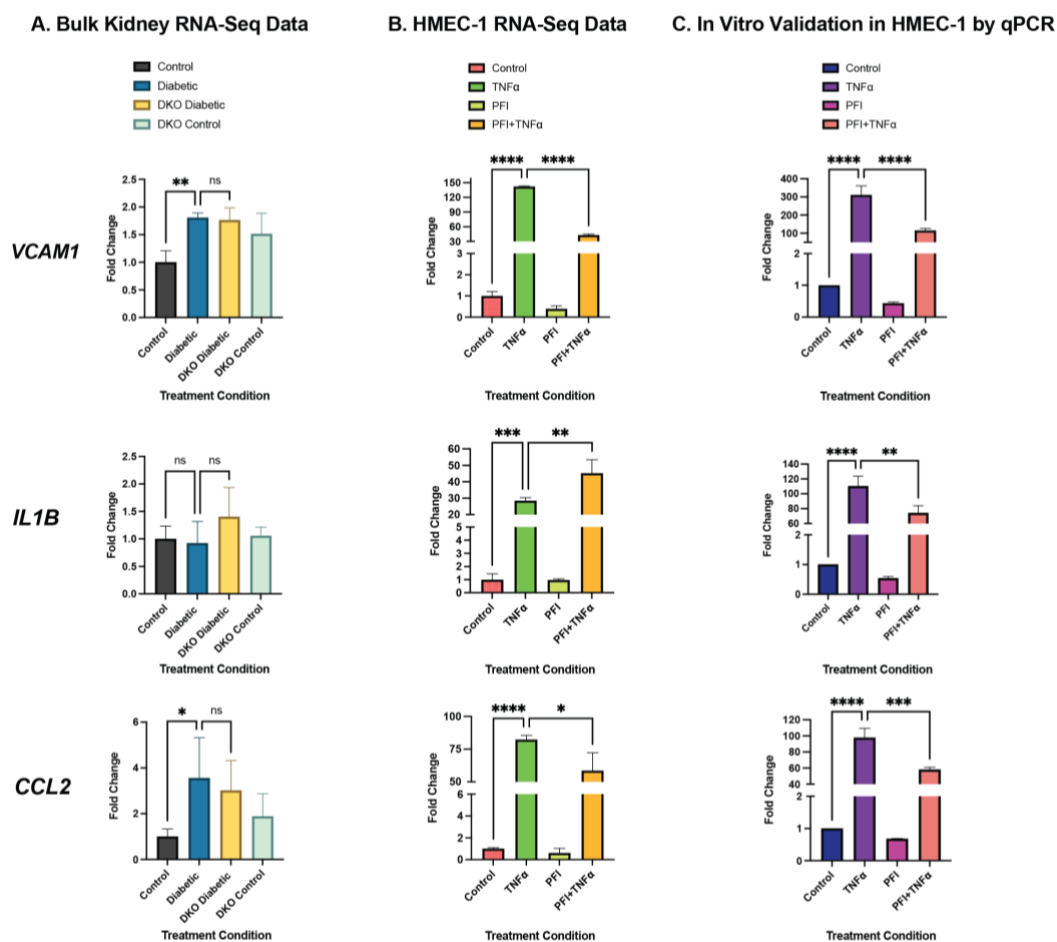


Figure 7: Set7 inhibition attenuates gene expression of inflammatory mediators

HMEC-1 cells were treated with 15 μ M (R)-PFI-2 and stimulated with TNF α for 72 hours. Quantification of mRNA levels was completed by RT-qPCR. H3F3A was used as a reference gene. n=3 per group. * p < 0.05, ** p < 0.01, *** p < 0.001 and **** p < 0.0001 (C). Gene expression profiles of genes associated with inflammation in three different data sets: bulk RNA-seq diabetic mouse kidney (A), RNA-Seq of HMEC-1 treated with TNF α and (R)-PFI-2 (B), and *in vitro* validation of gene expression changes conferred by Set7 inhibition in HMEC-1 cell culture (C).

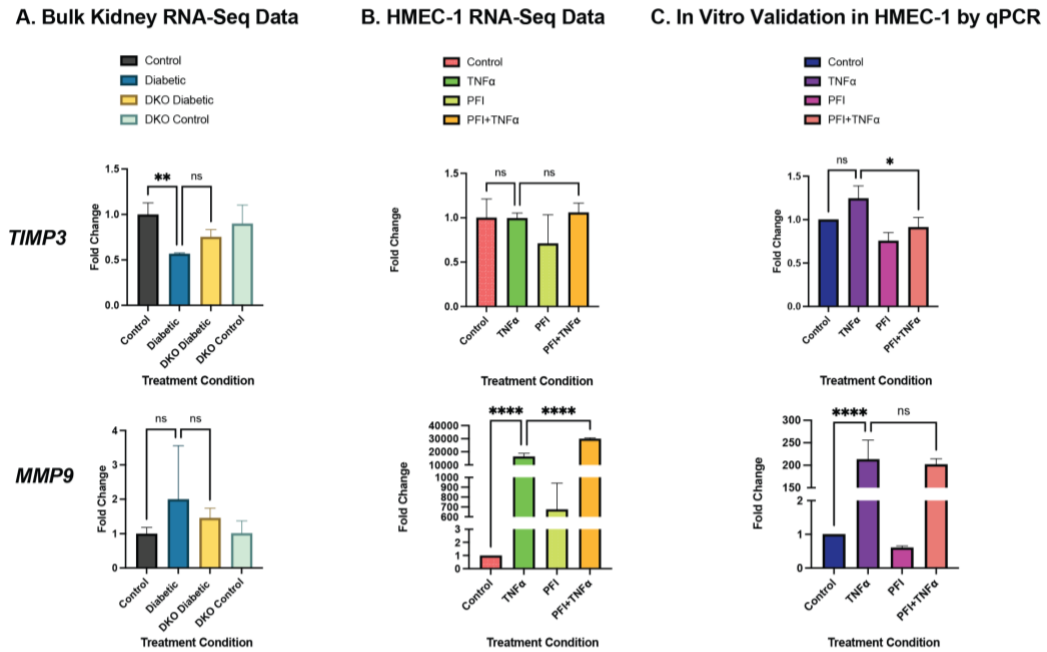


Figure 8: Gene expression profiles implicated in the extracellular matrix regulation

HMEC-1 cells were treated with 15 μ M (R)-PFI-2 and stimulated with TNF α for 72 hours. Quantification of mRNA levels was completed by RT-qPCR. H3F3A was used as a reference gene. n=3 per group. * p < 0.05, ** p < 0.01, *** p < 0.001 and **** p < 0.0001 (C). Gene expression profiles of genes associated with inflammation in three different data sets: bulk RNA-seq diabetic mouse kidney (A), RNA-Seq of HMEC-1 treated with TNF α and (R)-PFI-2 (B), and *in vitro* validation of gene expression changes conferred by Set7 inhibition in HMEC-1 cell culture (C).

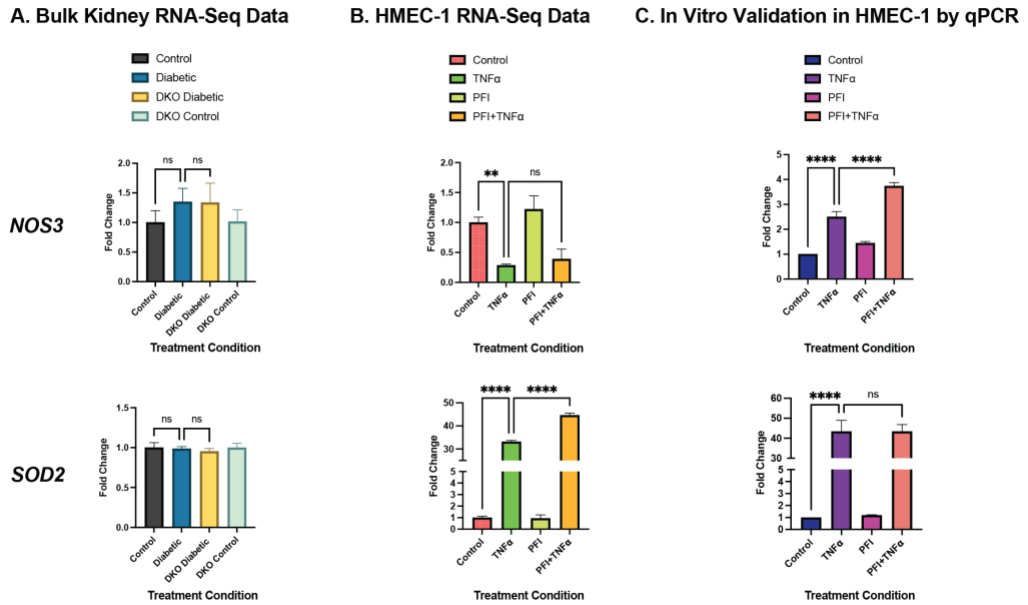


Figure 9: Gene expression profiles associated with vascular oxidative stress

HMEC-1 cells were treated with 15 μ M (R)-PFI-2 and stimulated with TNF α for 72 hours. Quantification of mRNA levels was completed by RT-qPCR. H3F3A was used as a reference gene. n=3 per group. * $p < 0.05$, ** $p < 0.01$, *** $p < 0.001$ and **** $p < 0.0001$ (C). Gene expression profiles of genes associated with inflammation in three different data sets: bulk RNA-seq diabetic mouse kidney (A), RNA-Seq of HMEC-1 treated with TNF α and (R)-PFI-2 (B), and *in vitro* validation of gene expression changes conferred by Set7 inhibition in HMEC-1 cell culture (C).

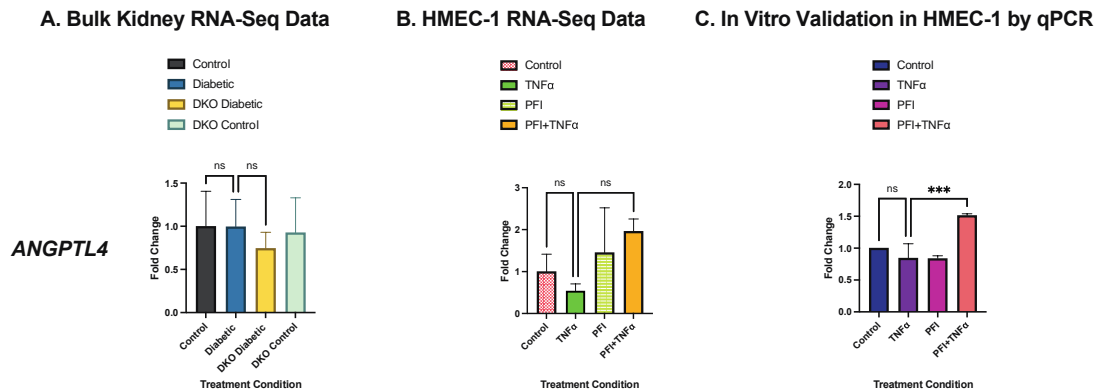


Figure 10: Gene expression profiles associated with lipid metabolism and cholesterol regulation

HMEC-1 cells were treated with 15 μ M (R)-PFI-2 and stimulated with TNF α for 72 hours. Quantification of mRNA levels was completed by RT-qPCR. H3F3A was used as a reference gene. n=3 per group. * p < 0.05, ** p < 0.01, *** p < 0.001 and **** p < 0.0001 (C). Gene expression profiles of genes associated with inflammation in three different data sets: bulk RNA-seq diabetic mouse kidney (A), RNA-Seq of HMEC-1 treated with TNF α and (R)-PFI-2 (B), and *in vitro* validation of gene expression changes conferred by Set7 inhibition in HMEC-1 cell culture (C).

4.6. Set7 inhibition alters patterns of H3K4me1 enrichment at several loci across VCAM1

VCAM1 is an inflammatory mediator that functions to regulate vascular cell adhesion and migration. Knowing that inflammation is a hallmark of diabetic endothelial dysfunction, we were prompted to further investigate this specific gene due to the prominence of its gene expression profile among the analysed data sets. *VCAM1* exhibited a significant increase in gene expression in both Diabetic vs. Control in the diabetic mouse kidney and TNF α vs. Control groups in HMEC-1 cells (Figure 7). Conversely, *VCAM1* was significantly downregulated in response to genetic and pharmacological inhibition of Set7. Our aim was to identify if the activity of the methyltransferase Set7 was in fact responsible for the downregulation of *VCAM1* expression in the experimental groups treated with the Set7-inhibiting agent, (R)-PFI-2. We assessed H3K4me1 using chromatin immunoprecipitation (ChIP), on chromatin isolated from HMEC-1 cells treated with TNF α and (R)-PFI-2. The UCSC Genome Browser (<https://genome.ucsc.edu/cgi-bin/hgPcr>) was used to identify H3K4 monomethylated regions along *VCAM1*. Primers were designed accordingly, ensuring that they were aligned with H3K4me1 peak regions, as well as reported enhancer regions. Our results showed significant decrease in H3K4me1 enrichment at *VCAM1* P2-region in response to (R)-PFI-2 (Figure 11). TNF α significantly increased H3K4me1 enrichment by 33% (***) $p < 0.001$) and treatment with PFI in the PFI + TNF α group significantly reversed the H3K4me1 enrichment (**** $p < 0.0001$) (Figure 11). Interestingly, this region is aligned with a reported enhancer region upstream of the gene *VCAM1* and is reported to interact with the promoter region of *VCAM1*. This interaction between regulatory elements indicates that Set7 could be responsible for the

alteration of the gene expression profile of *VCAMI* in diabetic conditions. Furthermore, no significant decrease in H3K4me1 enrichment had occurred in response to (R)-PFI-2 (Figure 12). Some regions showed decreased H3K4me1 at *VCAMI* (Regions - P3, P5, P6, P8, P11), however, statistical analysis listed these changes as not significant.

Our results are promising and reveal that pharmacological Set7 inhibitors play a role in the modulation of gene expression in human microvascular endothelial cells. Manipulation of the enzymatic activity of Set7 could provide a platform for attenuating TNF α -induced vascular inflammation via histone mechanisms and assessing pharmacological anti-inflammatory therapeutics in diabetic complications.

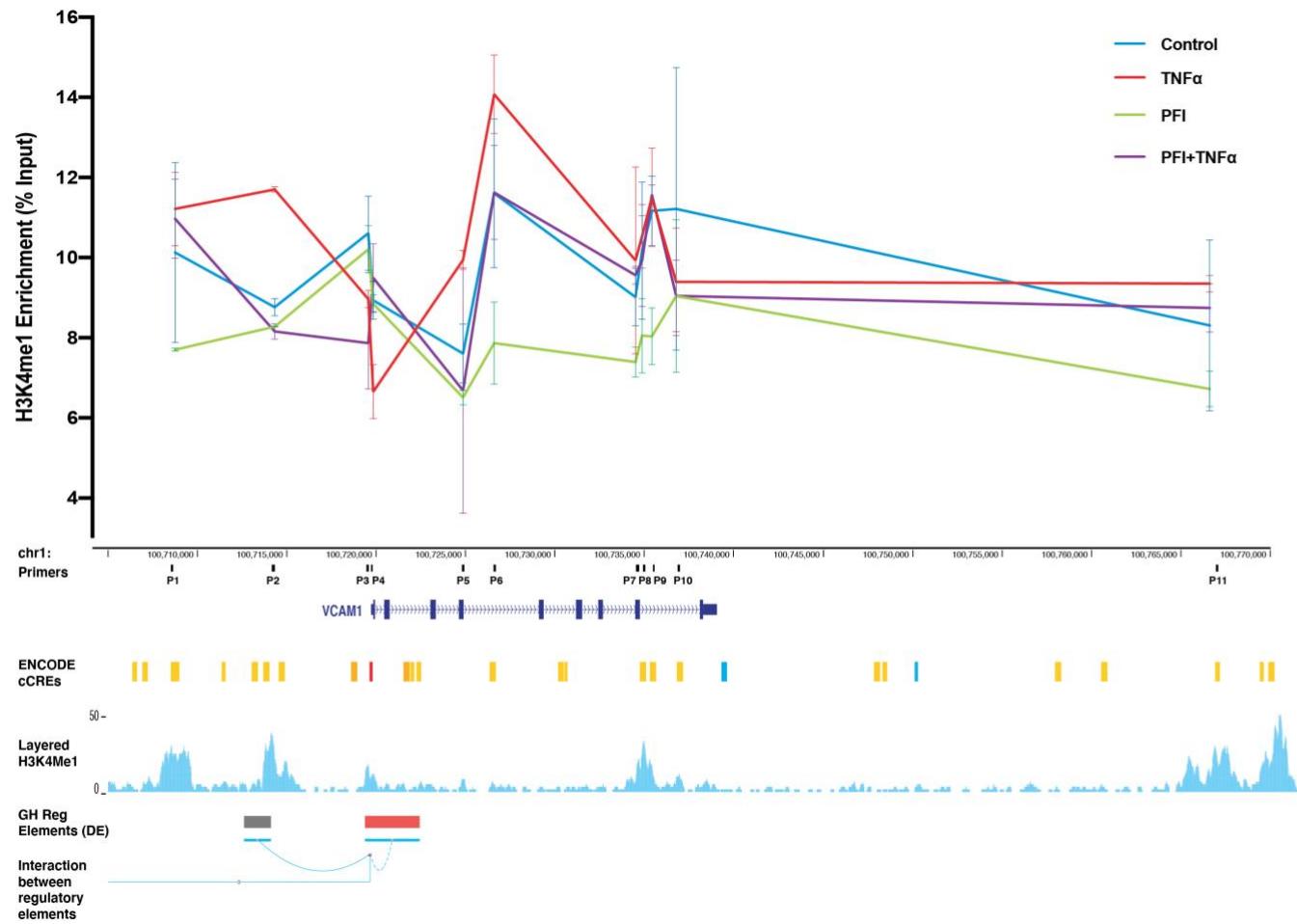


Figure 11: Comprehensive overview of H3K4me1 enrichment along VCAM1

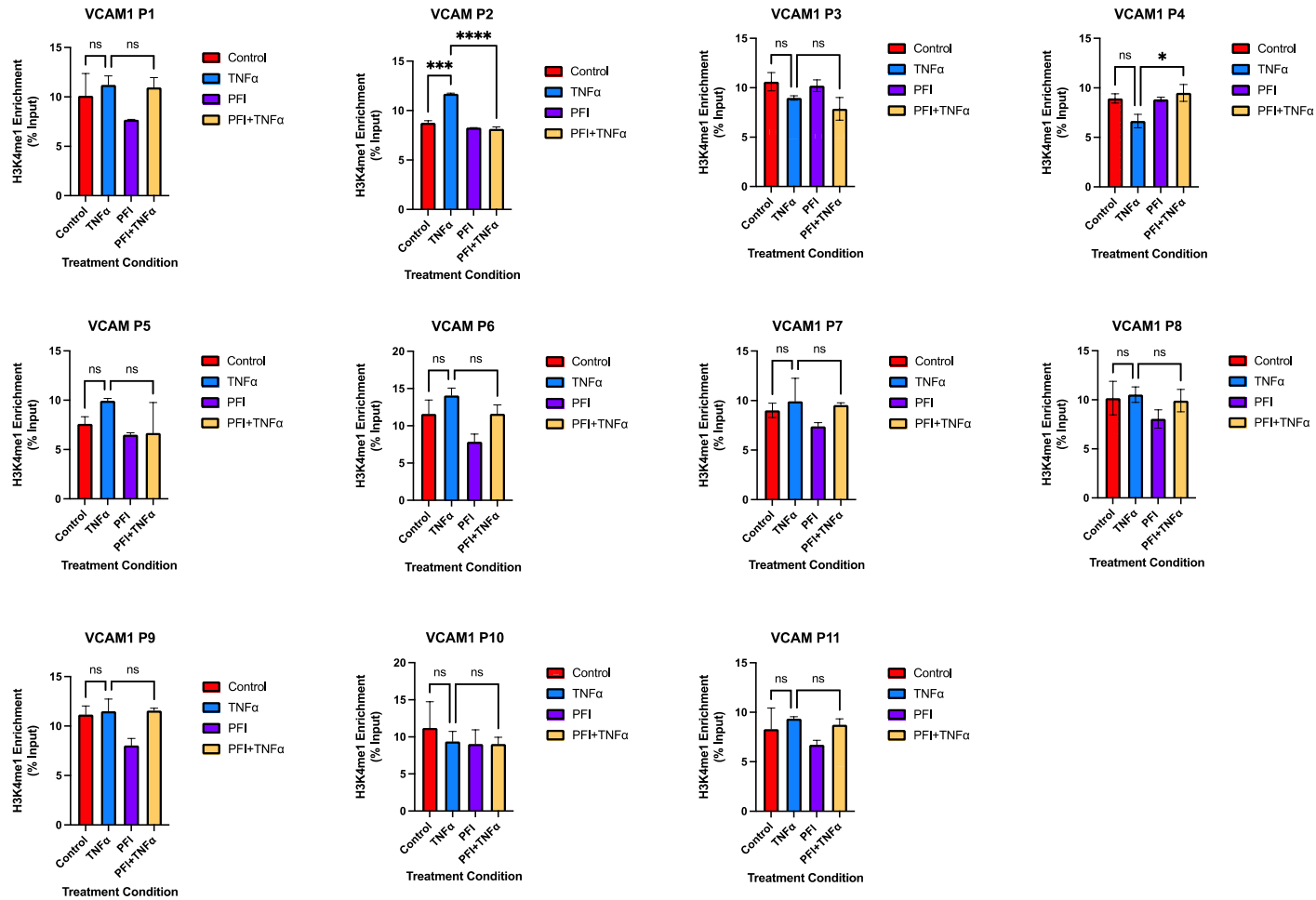


Figure 12: H3K4me1 enrichment levels of genomic regions along VCAM1 computed from RT-qPCR data to investigate association between Set7 inhibition and gene regulation

Figure 11: Comprehensive overview of H3K4me1 enrichment along VCAM1

Primers were designed along genomic regions of *VCAM1* that display peaks in H3K4me1 enrichment. Computation of RT-qPCR data using the % input method was reflective of the effects of Set7 inhibition and gene regulation of *VCAM1* through analysis of changes in H3K4me1 enrichment. *VCAM1* P2 showed significant reduction in H3K4me1 enrichment in the TNF α and (R)-PFI-2 treated group and this region is reported to interact with the promoter region of *VCAM1*, hence leading to the possibility of Set7 regulating the gene expression of *VCAM1* in inflammatory conditions.

Figure 12: H3K4me1 enrichment levels of genomic regions along VCAM1 computed from RT-qPCR data to investigate association between Set7 inhibition and gene regulation

Extracted chromatin from HMEC-1 cells treated with TNF α and (R)-PFI-2 were subjected to chromatin immunoprecipitation and incubated with a H3K4me1 antibody. The experimental setup consisted of the groups: input (control) and antibody (H3K4me1). RT-qPCR was performed with primers specifically designed for genomic regions along the gene *VCAM1* and data was analysed using the % input calculation method ($\% \text{ Input} = 100 \times 2^{(\text{Adjusted input} - \text{Ct of specific Ab})}$). n=2 per group. * p < 0.05, ** p < 0.01, *** p < 0.001 and **** p < 0.0001

CHAPTER 5

DISCUSSION

The endothelium plays a crucial role in the maintenance of vascular homeostasis. Physiological functions of the endothelium include leukocyte extravasation, regulation of thromboresistance, and ensuring adequate blood flow via modulation of vascular tone (Sena et al., 2013). However, imbalances in these regulatory mechanisms can result in the genesis of endothelial dysfunction. Altered physiological states that induce the cascade of events culminating to endothelial dysfunction include altered glucose homeostasis, chronic inflammation, and increased production of reactive oxygen species (ROS) (Hartge, Unger, & Kintscher, 2007). Diabetes-induced endothelial dysfunction is a gateway to the genesis of diabetic vascular complications and disease, such as cardiovascular disease (Gamrat, Surdacki, Chyrchel, & Surdacki, 2020). Therefore, building an understanding and exploring possible therapeutic approaches towards endothelial dysfunction is essential in the prevention of vascular complications in a diabetic setting.

Histone lysine methylation is a key contributor to transcriptional regulation, and consequently gene expression regulation. The histone methyltransferase, Set7, modifies chromatin by monomethylation of the lysine residue 4 of histone 3 (H3K4me1). Emergence of recent experimental evidence has established links between post-translational modifications (PTMs) and gene deregulation within the scope of pathological diseases, such as diabetes (Keating & El-Osta, 2013). Loss-of-function studies have successfully demonstrated how Set7 directs changes in gene expression

profiles in experimental models of human microvascular endothelial cells (HMEC-1) where over 8,000 genes were differentially dysregulated (Keating et al., 2014).

Identification of pharmacological selective inhibitors of Set7 have aided the investigation into the association of its molecular activity and regulating gene expression. Recognition of the capability of (R)-PFI-2, a Set7 inhibitor, has improved the feasibility to study the regulatory activity of this enzyme (Barsyte-Lovejoy et al., 2014). To further our overall understanding of these mechanistic links and gain additional insight into the underlying molecular mechanisms governing such epigenetic modifications in endothelial dysfunction, we assessed the effects of Set7 inhibition on the regulation of the endothelial transcriptome in diabetic inflammatory conditions.

Pathway analysis using RNA-sequencing in diabetic mouse kidney distinguished gene expression patterns in Set7 genetic inhibition (Figure 5). GSEA showed dysregulation in a wide array of biological pathways, where genes involved in regulatory cell processes exhibited prominent changes. Genes in pathways associated with endothelial dysfunction, which include vascular inflammation, extracellular matrix (ECM) dysregulation, oxidative stress, and altered lipid metabolism, were assessed. In diabetic mice, top pathways that were upregulated and subsequently reversed in Set7 KO include cytokine activity, carboxylic acid binding, inflammatory response, oxidoreductase activity, regulation of peptidase activity, and negative regulation of hydrolase activity. These pathways are fundamental contributors to the onset and persistence of chronic systemic inflammation (Charlton, Garzarella, Jandeleit-Dahm, & Jha, 2020; Fingleton, 2017). Gene-specific analysis of these pathways identified key genes implicated in each of the pathways (*VCAM1*, *IL1B*, *CCL2*, *TIMP3*, *MMP9*, *NOS3*,

SOD2, and *ANGPTL4*) and demonstrated the overall effect of *Set7* inhibition on genome-wide transcriptional regulation.

Analysis of the endothelial transcriptome in the HMEC-1 data set examined the role of pharmacological *Set7* inhibitors, specifically (R)-PFI-2, in the transcriptional regulation of TNF α -dependent gene expression in HMEC-1 cells. Pathway analysis revealed altered gene expression profiles in response to TNF α stimulation and the subsequent ability of PFI to reduce TNF α -activated gene expression (Figure 6), specifically of those involved in the inflammatory response such as cytokine and chemokine signalling (Figure 7.B and C). GSEA and *in vitro* validation revealed that TNF α upregulated gene expression of adhesion molecules and pro-inflammatory cytokines. In standard physiological conditions, PFI significantly reduced the gene expression of inflammatory mediators *VCAM*, *IL1B*, and *CCL2*. Moreover, in TNF α stimulated conditions, (R)-PFI-2 was able to reverse TNF α -induced gene expression of *VCAM1* and *CCL2*, but not of *IL1B* as also observed in the diabetic mouse kidney. On the other hand, the expression of *TIMP3*, *MMP9*, *NOS3*, *SOD2*, and *ANGPTL4* implicated in endothelial dysfunction were also altered by TNF α and but responded in unanticipated manner to pharmacological inhibition of *Set7*. Targeted pharmacological *Set7* inhibition showed attenuation of inflammatory signalling cascades and suggests TNF α -mediated activation of inflammatory and immune responses in human microvascular endothelial cells may be dependent on the activity of *Set7*. Importantly, our findings demonstrated a degree of correlation between TNF α -mediated genome-wide expression and diabetic mouse kidney RNA profiles.

We also observed some inconsistency in response to (R)-PFI-2 inhibition between HMEC-1 findings and mouse diabetic kidney. This could be attributed to specific experimental conditions of each data set. Firstly, the RNA-seq data of the diabetic mouse kidney is comprised of bulk kidney tissue, meaning that numerous cell types exist within the tissue extract. Gene expression changes are therefore representative of the combination of cell subtypes rather than a single cell type. On the other hand, the RNA-seq data of treated HMEC-1 cells solely reflects the gene expression changes of one specific cell type. Also, the mode of induction of diabetic conditions in animals could be a causal factor of variation between gene expression trends. Mouse models were administered streptozotocin (STZ) which is toxic to pancreatic B-cells that are responsible for producing insulin, whereas HMEC-1 models were treated with TNF α to induce inflammation which is another pathophysiological feature of diabetes. So, it can be clearly noted that each data set reflects two distinct characteristic conditions of diabetes and perhaps could be explain the differences. Lastly, the method used to inhibit Set7 also differs between both experiments; the diabetic mouse kidney was subjected to Set7 knockout whereas HMEC-1 cells were treated with the Set7-inhibiting drug, (R)-PFI-2. Recent studies have presented experimental evidence showing that Set7 may be accompanied by other histone methyltransferases in writing mono-methylation of H3K4 (Keating et al., 2014). This raises the possibility of the involvement of compensatory enzymes in the complete absence of Set7 in the genetic knock-out model. All things considered; the listed reasons serve as limitation in comparing gene expression patterns among the data sets.

Quantitative analysis of *in vitro* validation of gene expression in HMEC-1 cells was completed and figures were generated from the previously analysed RNA-seq data sets, bulk mouse kidney RNA-seq and HMEC-1 RNA-seq (Figures 7, 8, 9, and 10), to conduct a comparative analysis and assess consistency of then data trends among the three data sets. The set of genes selected from the RNA-seq data sets were grouped according to their biological function: inflammation (Figure 7.), extracellular matrix regulation (Figure 8.), oxidative stress mediators (Figure 9.), and lipid metabolism (Figure 10.).

Inflammation is a hallmark of endothelial dysfunction in diabetes mellitus. Pathophysiological mechanisms associated with the onset of diabetes trigger the release of inflammatory mediators, such as cytokines, in response to the deviation from glucose homeostasis. Prolonged activation of immune responses associated with inflammation can be harmful to cells. For instance, persistent inflammation in a diabetic milieu is a primary cause of endothelial dysfunction and cardiovascular disease (Castellon & Bogdanova, 2016; Steyers & Miller, 2014). TNF α is a recognized cytokine that has significant role in eliciting inflammatory responses and inducing robust immune responses (Croft et al., 2012; Horiuchi, Mitoma, Harashima, Tsukamoto, & Shimoda, 2010). Responses stimulated by this pro-inflammatory cytokine are precursors of endothelial dysfunction, thus it was ideal to use as a stimulant in our study (Kleinbongard, Heusch, & Schulz, 2010; Mudau, Genis, Lochner, & Strijdom, 2012; Steyers & Miller, 2014).

GSEA of the RNA-seq data of the diabetic mouse kidney showed positive enrichment of inflammatory response and cytokine activity pathways. Of clinical significance, the overactivity of cytokines and inflammatory mediators is associated with dysfunctional cellular activity. Genes exhibiting prominent roles in inflammatory and immune responses included in the GSEA pathways are *VCAMI*, *IL1B*, and *CCL2*, which were upregulated in inflammatory conditions (TNF α and Diabetic groups) (Figure 7.)

Upregulation of the vascular cell adhesion molecule 1 (*VCAMI*) is a phenotypic feature of endothelial dysfunction (Habas & Shang, 2018). *VCAMI* is critical in mediating leukocyte adhesion and trans-endothelial migration (Abdala-Valencia, Berdnikovs, & Cook-Mills, 2011). Progression of atherosclerosis is closely linked to mechanisms of vascular inflammation and endothelial dysfunction (Petrie, Guzik, & Touyz, 2018). It has been reported that *VCAMI* is highly expressed throughout the formation of atherosclerotic plaque and plays a prominent role in the progression of atherosclerosis via compromising the integrity of the endothelial lining of blood vessels (Cook-Mills, Marchese, & Abdala-Valencia, 2011). Analysis of the TNF α -stimulated gene expression profile of *VCAMI* in HMEC-1 cells exhibited a significant increase in *VCAMI* expression, as well as in the diabetic mouse model. This data corroborates a previous report which showed the upregulation of *VCAMI* in endothelial cells in the presence of TNF α (J. X. Yang et al., 2016). In response to Set7 inhibition, *VCAMI* expression was significantly attenuated in HMEC-1 cells. It is essential to understand the underlying mechanisms pertaining to the function of *VCAMI* signalling in inflammation and disease progression to develop an approach to modulate *VCAMI*-dependent inflammation in endothelial dysfunction. Our results suggest a role for Set7

in gene regulation of *VCAMI* and possibly lead to an anti-inflammatory therapeutic approach in diabetic settings through pharmacological inhibition of Set7 using (R)-PFI-2.

In addition to *VCAMI*, increased gene expression of pro-inflammatory cytokines is implicated in the genesis of vascular endothelial dysfunction and cardiovascular disease. Substantial expression of *IL1B* is characteristic of atherosclerotic lesions and it has been demonstrated that pharmacological intervention reduced development and progression of atherosclerosis (Bhaskar et al., 2011; Chamberlain et al., 2006). Interleukin 1- β (*IL-1 β*) is a pro-inflammatory cytokine that is responsible for reinforcing auto-inflammatory cellular signalling, thus further exacerbating development of complications. The interleukin family is categorized based on their ability to either augment or inhibit an inflammatory response. Pro-inflammatory interleukins include IL-1, IL-2, IL-6, IL-7, IL-8, IL-15, IL-17, and IL-18, whereas anti-inflammatory interleukins include IL-4, IL-10, IL-11, IL-12, and IL13 (Peiro, Lorenzo, Carraro, & Sanchez-Ferrer, 2017). Mounting evidence has demonstrated the increased expression of *IL-1 β* in hyperglycaemic and inflammatory conditions (Holmes, 2017), which was expectedly detected in our TNF α -stimulated HMEC-1 RNA-seq pathway analysis (Figure 7.B). Malfunctioning of the vascular endothelium is an early manifestation and precursor of vascular disease. Upregulation of pro-inflammatory cytokines have been shown to be dominantly expressed in atherosclerotic lesions of *in vitro* and *in vivo* models (Liu et al., 2014). Endothelial dysfunction evoked by *IL-1 β* plays a key role in the development of cardiovascular complications, hence establishing a therapeutic approach that aims to reduce its expression and prevent progression of the disease is an ideal objective. Pharmacological inhibition of *IL-1 β* has been successfully achieved and

approved for clinical use in recent years. These drugs include Anakira, an IL-1R α receptor antagonist, Rilonacept, a soluble decoy receptor, and Canakinumab, a monoclonal anti-IL-1 β that neutralizes soluble IL-1 β (Dinarello, Simon, & van der Meer, 2012). Our results show that Set7 inhibition could provide a novel alternative approach through targeting epigenetic modifications, rather than intracellular signalling mechanisms. Consistent with these reports, GSEA pathway analysis and *in vitro* validation of gene expression profiles in HMEC-1 cells showed a reversal in IL-1 β expression in the Set7-inhibited models, using the pharmacological agent (R)-PFI-2. Although further study would be required, our findings provide a possible approach in attenuating diabetes-induced chronic inflammation by targeting this pro-inflammatory cytokine and thus delaying the onset of atherosclerotic manifestations.

The pro-inflammatory chemokine, chemokine (C-C motif) ligand 2 (*CCL2*), is also associated with endothelial dysfunction. It is also known as monocyte chemoattractant protein (MCP-1). The CCL2/CCR2-axis is responsible for the mediation of monocyte chemotaxis and extravasation upon exposure to inflammatory stimuli, such as TNF α (Gschwandtner, Derler, & Midwood, 2019). Excessive monocyte infiltration results in exacerbation of vascular diabetic complications. Recruitment of monocytes to sites of inflammation, such as developing atherosclerotic lesions, influences the progression of atherosclerosis (Noels, Weber, & Koenen, 2019). In this study, diabetic settings increased *CCL2* gene expression in both TNF α -stimulated HMEC-1 cells and diabetic mouse kidney. We detected reduction of TNF α -induced and STZ-induced gene expression of *CCL2* by Set7 inhibition. Taken together, our data highlights the competence of (R)-PFI-2 to regulate inflammation-induced gene expression.

In response to inflammatory insults to the endothelium, endothelial cells release a wide array of inflammatory mediators and growth factors that could be a contributor to ECM deposition and remodelling (Sziksz et al., 2015). MMPs are a family of proteolytic enzymes that are responsible for the degradation of ECM components such as collagen, proteoglycans, and elastin. MMPs play a key role in vascular remodelling, in which they have the ability to alter blood vessel size and composition. These regulatory processes are crucial in dictating vessel plasticity and repair. Excessive secretion of these proteolytic enzymes can lead to dysregulated vascular remodelling and atherosclerosis. Previous research has demonstrated the presence of MMPs in atherosclerotic plaques and in regions proximal to foam cell clusters (Olson et al., 2008). The modulation of MMP expression is critical to the regulation of their overactivity and therefore cardiovascular disease progression. In a previous study, overexpression of *MMP9* has been shown to directly affect endothelial cells where it exerts pro-apoptotic and pro-inflammatory properties through enzyme activation of a classical thrombin receptor expressed on vascular endothelial cells, protease activated receptor-1 (PAR-1) (Florence, Krupa, Booshehri, Allen, & Kurdowska, 2017). Proteinase inhibitors, known as tissue inhibitors of metalloproteinases (TIMPs), regulate the activity of MMPs. Overexpression of MMPs is postulated to be linked to unbalanced expression of TIMPs. Imbalances in the MMP-TIMP ratio, that favour increased ECM degradation, may promote the development of diabetic-induced atherosclerosis. Reported findings have detected decreased expression of *TIMP3* in atherosclerotic plaques in patients with type 2 diabetes (Cardellini et al., 2009). We aimed to investigate the capacity of (R)-PFI-2 to attenuate TNF α -activated gene expression of genes implicated in ECM regulation, MMP9 and TIMP3. Set7 inhibition

was able to attenuate *MMP9* expression in the diabetic mouse model and the *in vitro* validation in TNF α -stimulated HMEC-1 cells, however HMEC-1 RNA-seq reported increased expression. RNA-seq data sets of both diabetic mouse kidney and TNF α -stimulated HMEC-1 cells demonstrated decreased TIMP3 expression in diabetic inflammatory conditions, consistent with published findings. On the contrary, *in vitro* validation in HMEC-1 cells detected increased *TIMP3* expression in the TNF α -stimulated group. Previous research has demonstrated that overexpression of *TIMP3* results in a decreased inflammatory response and progression of atherosclerotic plaques in mice (Casagrande et al., 2012). *Set7* inhibition using genetic knockout resulted in upregulation of *TIMP3* whereas pharmacological inhibition using (R)-PFI-2 did not demonstrate the expected increase in gene expression. These results provide a promising approach to reducing vascular complications of endothelial dysfunction, however the exact effect of *Set7* activity on the regulation of these genes remains obscure based on obtained results. Interestingly, the concurrent attenuation of *MMP9* and *TIMP3* by *Set7* inhibition could prove to be valuable in re-establishing normal regulatory conditions of the extracellular matrix and restoring the MMP-TIMP ratio, thus hindering progression of atherosclerosis. Additional study is required to solidify this postulation and rule out possibilities of technical errors and data discrepancies.

Oxidative stress, resulting from an imbalance of the production and degradation of reactive oxygen species (ROS), has been shown to be a possible contributor to endothelial dysfunction and atherosclerosis. The endothelial NOS (eNOS) enzyme, also known as nitric oxide synthase 3 (NOS3), is encoded by the *NOS3* gene. It has been reported to possess anti-atherosclerotic functions, such as the production of the vasodilatory agent nitric oxide (NO), inhibition of platelet aggregation, and limits

immune cell adhesion (Schulz, Gori, & Munzel, 2011). Reduced endothelium-dependent relaxations (EDR), induced by NO, are present in atherosclerotic vessels due to the likely cause of the reduced bioavailability of NO (Kawashima & Yokoyama, 2004). Decreased eNOS expression has been postulated to be a cause of endothelial dysfunction, however several studies show the opposite (Forstermann & Munzel, 2006). Studies have shown that eNOS deficiency accelerates the formation of atherosclerotic lesions (Oemar et al., 1998). Conversely, in studied atherosclerotic animal models with impaired EDR, an increased expression of eNOS was reported (d'Uscio, Smith, & Katusic, 2001). This duplicitous nature of eNOS may result from tetrahydrobiopterin (BH4) metabolism, a cofactor of eNOS (Kawashima & Yokoyama, 2004). A level of ambiguity surrounds the exact role of eNOS in endothelial dysfunction and our findings also exhibited contrasting results between the data sets. NOS3 gene expression was upregulated in the diabetic mouse kidney and showed no significant change in response to Set7KO. TNF α -stimulation in HMEC-1 cells resulted in decreased NOS3 expression in the RNA-seq data set, however it was increased in RT-qPCR validation; (R)-PFI-2 augmented *NOS3* expression in both HMEC-1 data sets relative to the control. We also examined the gene expression of the superoxide dismutase 2 (*SOD2*), an antioxidant enzyme involved in protecting the endothelium against oxidative stress. *SOD2* functions as a ROS scavenger by degrading mitochondrial reactive oxygen species. Based on experimental evidence, it has been reported that reduced *SOD2* expression results in endothelial dysfunction, however the exact nature and validity of this association remains ambiguous (Ohashi, Runge, Faraci, & Heistad, 2006; Tseng et al., 2017). Based on our computed results, *SOD2* gene expression was increased in response to TNF α and showed little to no change in the (R)-PFI-2 treated groups. A possible

justification of the overexpression of *SOD2* could be that it is eliciting a protective reaction in response to TNF α to prevent further hyperglycaemic injury to endothelial cells. Conversely, experimental error could be the culprit of the generated gene expression profiles; nevertheless, further study is required to eliminate this ambiguity.

Moreover, a notable manifestation of endothelial dysfunction and cardiovascular complications includes altered lipid metabolism. Dyslipidaemia and lipid-driven chronic inflammation has been shown to induce endothelial dysfunction and thus aggravate the pathological progression of atherosclerotic cardiovascular events (Ghosh, Gao, Thakur, Siu, & Lai, 2017). In our study, we examined a key gene involved in the regulation of lipid metabolism, angiopoietin-like 4 (*ANGPTL4*). *ANGPTL4* plays a vital role in lipid metabolism through its inhibition of lipoprotein lipase (LPL) activity. LPL is an enzyme that is responsible for mediating triglyceride hydrolysis, where its activation results in lowered levels of circulating triglycerides-rich lipoproteins. Evidence pertaining to the exact nature of the atherogenicity of this enzyme remains inconclusive; it has been claimed to have both an anti-atherogenic and pro-atherogenic effect, however further study is required to understand its functionality (Kobayashi & Mabuchi, 2015). *ANGPTL4* has also been claimed to play a role in maintenance of endothelial cell integrity by regulating vascular permeability. Loss of endothelial cell integrity is a precursor of endothelial dysfunction and subsequent initiation of atherogenesis (Xu et al., 2015). In spite of this, controversy surrounds whether its role is beneficial or detrimental to endothelial cells. Studies have shown that it can be destructive to the endothelium (Huang et al., 2011), whereas others have shown that it exerts a protective role (Galaup et al., 2012). It has also been reported that *ANGPTL4* expression is influenced by tissue-specificity and nutritional states; it is upregulated in

fasted conditions and downregulated in obesity and consumption of a high-fat diet (Dutton & Trayhurn, 2008; J. Yang, Li, & Xu, 2021). The role of *ANGPTL4* in endothelial dysfunction remains unclear. Our results illustrated a downregulation of *ANGPTL4* expression in TNF α -stimulated conditions and an upregulation in both standard physiological and TNF α -induced inflammatory conditions treated with (R)-PFI-2. Our findings are consistent with the hypothesized downregulation of *ANGPTL4* in a hyperlipidemic milieu.

As mentioned, gene expression trends are show a degree of inconsistently between HMEC-1. The discrepancy between the HMEC-1 data set and the *in vitro* validated gene expression profiles by RT-qPCR could possibly be because RNA-sequencing reads the entire span of the gene, whereas the RT-qPCR data only exhibits gene expression patterns of a specific primer region; however, this warrants further investigation.

As previously discussed, the pro-inflammatory gene, *VCAM1*, is of great importance regarding its role in diabetes-induced inflammatory responses. Analysis of the histone modification changes mediated by Set7, H3K4 monomethylation, along the gene *VCAM1* was assessed using chromatin immunoprecipitation (ChIP) to investigate the effect of (R)-PFI-2 on H3K4me1 enrichment in TNF α -stimulated conditions. Interestingly, a region upstream of *VCAM1*, labelled as *VCAM1* P2 in our results (Figure 11-12), showed a significant decrease in H3K4me1 enrichment in response to (R)-PFI-2. This specific genomic locus happens to be of proximity to a reported regulatory enhancer region that interacts with the promoter region of *VCAM1* (Fishilevich et al., 2017; Stelzer et al., 2016). Decreased H3K4me1 enrichment correlates with transcriptional repression of *VCAM1* as shown in RNA-seq and RT-

qPCR results of the studied data sets. Thus, the observed interaction between regulatory elements signifies that the alteration of the gene expression profile of *VCAMI* in diabetic inflammatory conditions is mediated by Set7. Moreover, no other significant decreases in H3K4me1 enrichment were not detected in response to (R)-PFI-2 (Figure 11.). These results provide evidence for Set7-dependent gene regulation occurring at specific loci, rather than recurrently at multiple loci along the gene. Previous studies examining *VCAMI* inhibition directly and indirectly by targeting downstream signalling proteins, NADPH oxidase, protein kinase C α (PKC α), and protein tyrosine phosphatase 1B (PTP1B) has shown to attenuate transendothelial migration of leukocytes induced by *VCAMI* (Abdala-Valencia et al., 2011). In comparison to previous experimental approaches to inhibit *VCAMI* expression, our alternative approach through targeting histone-dependent mechanisms could provide a direct therapeutic effect, prior to the initiation of associated signalling cascades. Importantly, these findings demonstrate Set7-mediated transcriptional regulation by modifying H3K4me1 enrichment at distinct loci along certain genes, consistent with past reports that have exemplified the influential role of Set7 monomethylation on gene regulation (Brasacchio et al., 2009; Keating & El-Osta, 2013). Overall, pharmacological inhibition of Set7 using (R)-PFI-2 could prove to be highly beneficial in attenuating the transcriptional activation of pro-inflammatory *VCAMI*, thus opposing vascular inflammation in endothelial cells.

CHAPTER 6

CONCLUSION

In conclusion, the present study highlights the role of Set7-mediated transcriptional regulation and the effect of pharmacological Set7 inhibition on the mediation of gene expression profiles in human microvascular endothelial cells. Robust genome-wide changes were identified using RNA-sequencing in TNF α -stimulated HMEC-1 cells and ApoE KO Set7 KO STZ-treated mice. GSEA analysis illustrated significant genome-wide upregulation of pathways implicated in endothelial dysfunction, such as the inflammatory response and cytokine activity pathways. Reversal of these gene expression profiles was exemplified in genetically Set7-inhibited groups.

TNF α stimulation resulted in gene dysregulation within the endothelial transcriptome of HMEC-1 cells, expectedly due to the onset of inflammation and consequent immune responses. On the contrary, pharmacological Set7 inhibition using (R)-PFI-2 exhibited significant downregulation of gene expression profiles in HMEC-1 cells. We examined the role of Set7 in gene regulation in a variety of biological responses essential to maintaining homeostatic vascular function and thus the integrity of the endothelium. These include vascular inflammation, extracellular matrix dysregulation, oxidative stress, and altered lipid metabolism. Gene-specific expression profiles of *VCAM1*, *IL-1 β* , *CCL2*, *MMP9*, *TIMP3*, *NOS3*, *SOD2*, and *ANGPTL4* were experimentally assessed to identify alterations conferred by Set7 inhibition. Examination of H3K4me1 peaks at several loci along *VCAM1* revealed an interaction between regulatory gene elements, which provides a promising outlook to establishing a

role for Set7 in suppressing the inflammatory activity of this gene, and potentially others, through histone-dependent mechanisms.

Overall, results have emphasized the potential use of Set7 inhibition as a platform for a pharmacological anti-inflammatory therapeutic approach to attenuating vascular inflammation and diabetic endothelial dysfunction. Future experimental research will be required to consolidate our findings and provide further insight into the mechanistic links between Set7 activity and gene regulation in a diabetic inflammatory setting. Investigation of Set7-dependent non-histone methylation at could provide additional understanding of the functionality of Set7 and could perhaps be an alternative mode of gene regulation. Additionally, this can further determine the extent of involvement of histone-mediated regulation by Set7.

REFERENCES

- Abdala-Valencia, H., Berdnikovs, S., & Cook-Mills, J. M. (2011). Mechanisms for vascular cell adhesion molecule-1 activation of ERK1/2 during leukocyte transendothelial migration. *PLoS One*, *6*(10), e26706. doi:10.1371/journal.pone.0026706
- Bannister, A. J., & Kouzarides, T. (2011). Regulation of chromatin by histone modifications. *Cell Res*, *21*(3), 381-395. doi:10.1038/cr.2011.22
- Barski, A., Cuddapah, S., Cui, K., Roh, T. Y., Schones, D. E., Wang, Z., . . . Zhao, K. (2007). High-resolution profiling of histone methylations in the human genome. *Cell*, *129*(4), 823-837. doi:10.1016/j.cell.2007.05.009
- Barsyte-Lovejoy, D., Li, F., Oudhoff, M. J., Tatlock, J. H., Dong, A., Zeng, H., . . . Arrowsmith, C. H. (2014). (R)-PFI-2 is a potent and selective inhibitor of SETD7 methyltransferase activity in cells. *Proc Natl Acad Sci U S A*, *111*(35), 12853-12858. doi:10.1073/pnas.1407358111
- Beckman, J. A., & Creager, M. A. (2016). Vascular Complications of Diabetes. *Circ Res*, *118*(11), 1771-1785. doi:10.1161/CIRCRESAHA.115.306884
- Bhaskar, V., Yin, J., Mirza, A. M., Phan, D., Vanegas, S., Issafras, H., . . . Kantak, S. S. (2011). Monoclonal antibodies targeting IL-1 beta reduce biomarkers of atherosclerosis in vitro and inhibit atherosclerotic plaque formation in Apolipoprotein E-deficient mice. *Atherosclerosis*, *216*(2), 313-320. doi:10.1016/j.atherosclerosis.2011.02.026
- Brasacchio, D., Okabe, J., Tikellis, C., Balcerzyk, A., George, P., Baker, E. K., . . . El-Osta, A. (2009). Hyperglycemia induces a dynamic cooperativity of histone methylase and demethylase enzymes associated with gene-activating epigenetic marks that coexist on the lysine tail. *Diabetes*, *58*(5), 1229-1236. doi:10.2337/db08-1666
- Cardellini, M., Menghini, R., Martelli, E., Casagrande, V., Marino, A., Rizza, S., . . . Federici, M. (2009). TIMP3 is reduced in atherosclerotic plaques from subjects with type 2 diabetes and increased by SirT1. *Diabetes*, *58*(10), 2396-2401. doi:10.2337/db09-0280
- Casagrande, V., Menghini, R., Menini, S., Marino, A., Marchetti, V., Cavalera, M., . . . Federici, M. (2012). Overexpression of tissue inhibitor of metalloproteinase 3 in macrophages reduces atherosclerosis in low-density lipoprotein receptor knockout mice. *Arterioscler Thromb Vasc Biol*, *32*(1), 74-81. doi:10.1161/ATVBAHA.111.238402
- Castellon, X., & Bogdanova, V. (2016). Chronic Inflammatory Diseases and Endothelial Dysfunction. *Aging Dis*, *7*(1), 81-89. doi:10.14336/AD.2015.0803
- Chamberlain, J., Evans, D., King, A., Dewberry, R., Dower, S., Crossman, D., & Francis, S. (2006). Interleukin-1beta and signaling of interleukin-1 in vascular wall and circulating cells modulates the extent of neointima formation in mice. *Am J Pathol*, *168*(4), 1396-1403. doi:10.2353/ajpath.2006.051054
- Chan, J. C., & Maze, I. (2020). Nothing Is Yet Set in (Hi)stone: Novel Post-Translational Modifications Regulating Chromatin Function. *Trends Biochem Sci*, *45*(10), 829-844. doi:10.1016/j.tibs.2020.05.009

- Charlton, A., Garzarella, J., Jandeleit-Dahm, K. A. M., & Jha, J. C. (2020). Oxidative Stress and Inflammation in Renal and Cardiovascular Complications of Diabetes. *Biology (Basel)*, *10*(1). doi:10.3390/biology10010018
- Choudhuri, S., Cui, Y., & Klaassen, C. D. (2010). Molecular targets of epigenetic regulation and effectors of environmental influences. *Toxicol Appl Pharmacol*, *245*(3), 378-393. doi:10.1016/j.taap.2010.03.022
- Chuikov, S., Kurash, J. K., Wilson, J. R., Xiao, B., Justin, N., Ivanov, G. S., . . . Reinberg, D. (2004). Regulation of p53 activity through lysine methylation. *Nature*, *432*(7015), 353-360. doi:10.1038/nature03117
- Cook-Mills, J. M., Marchese, M. E., & Abdala-Valencia, H. (2011). Vascular cell adhesion molecule-1 expression and signaling during disease: regulation by reactive oxygen species and antioxidants. *Antioxid Redox Signal*, *15*(6), 1607-1638. doi:10.1089/ars.2010.3522
- Croft, M., Duan, W., Choi, H., Eun, S. Y., Madireddi, S., & Mehta, A. (2012). TNF superfamily in inflammatory disease: translating basic insights. *Trends Immunol*, *33*(3), 144-152. doi:10.1016/j.it.2011.10.004
- d'Uscio, L. V., Smith, L. A., & Katusic, Z. S. (2001). Hypercholesterolemia impairs endothelium-dependent relaxations in common carotid arteries of apolipoprotein e-deficient mice. *Stroke*, *32*(11), 2658-2664. doi:10.1161/hs1101.097393
- Dillon, S. C., Zhang, X., Trievel, R. C., & Cheng, X. (2005). The SET-domain protein superfamily: protein lysine methyltransferases. *Genome Biol*, *6*(8), 227. doi:10.1186/gb-2005-6-8-227
- Dinarello, C. A., Simon, A., & van der Meer, J. W. (2012). Treating inflammation by blocking interleukin-1 in a broad spectrum of diseases. *Nat Rev Drug Discov*, *11*(8), 633-652. doi:10.1038/nrd3800
- Dupont, C., Armant, D. R., & Brenner, C. A. (2009). Epigenetics: definition, mechanisms and clinical perspective. *Semin Reprod Med*, *27*(5), 351-357. doi:10.1055/s-0029-1237423
- Dutton, S., & Trayhurn, P. (2008). Regulation of angiopoietin-like protein 4/fasting-induced adipose factor (Angptl4/FIAF) expression in mouse white adipose tissue and 3T3-L1 adipocytes. *Br J Nutr*, *100*(1), 18-26. doi:10.1017/S0007114507882961
- El-Osta, A., Brasacchio, D., Yao, D., Poci, A., Jones, P. L., Roeder, R. G., . . . Brownlee, M. (2008). Transient high glucose causes persistent epigenetic changes and altered gene expression during subsequent normoglycemia. *J Exp Med*, *205*(10), 2409-2417. doi:10.1084/jem.20081188
- Esteve, P. O., Chin, H. G., Benner, J., Feehery, G. R., Samaranayake, M., Horwitz, G. A., . . . Pradhan, S. (2009). Regulation of DNMT1 stability through SET7-mediated lysine methylation in mammalian cells. *Proc Natl Acad Sci U S A*, *106*(13), 5076-5081. doi:10.1073/pnas.0810362106
- Ferrari, K. J., Scelfo, A., Jammula, S., Cuomo, A., Barozzi, I., Stutzer, A., . . . Pasini, D. (2014). Polycomb-dependent H3K27me1 and H3K27me2 regulate active transcription and enhancer fidelity. *Mol Cell*, *53*(1), 49-62. doi:10.1016/j.molcel.2013.10.030
- Fingleton, B. (2017). Matrix metalloproteinases as regulators of inflammatory processes. *Biochim Biophys Acta Mol Cell Res*, *1864*(11 Pt A), 2036-2042. doi:10.1016/j.bbamcr.2017.05.010

- Fishilevich, S., Nudel, R., Rappaport, N., Hadar, R., Plaschkes, I., Iny Stein, T., . . . Cohen, D. (2017). GeneHancer: genome-wide integration of enhancers and target genes in GeneCards. *Database (Oxford)*, 2017. doi:10.1093/database/bax028
- Florence, J. M., Krupa, A., Booshehri, L. M., Allen, T. C., & Kurdowska, A. K. (2017). Metalloproteinase-9 contributes to endothelial dysfunction in atherosclerosis via protease activated receptor-1. *PLoS One*, 12(2), e0171427. doi:10.1371/journal.pone.0171427
- Forstermann, U., & Munzel, T. (2006). Endothelial nitric oxide synthase in vascular disease: from marvel to menace. *Circulation*, 113(13), 1708-1714. doi:10.1161/CIRCULATIONAHA.105.602532
- Forstermann, U., Xia, N., & Li, H. (2017). Roles of Vascular Oxidative Stress and Nitric Oxide in the Pathogenesis of Atherosclerosis. *Circ Res*, 120(4), 713-735. doi:10.1161/CIRCRESAHA.116.309326
- Fyodorov, D. V., Zhou, B. R., Skoultchi, A. I., & Bai, Y. (2018). Emerging roles of linker histones in regulating chromatin structure and function. *Nat Rev Mol Cell Biol*, 19(3), 192-206. doi:10.1038/nrm.2017.94
- Galaup, A., Gomez, E., Souktani, R., Durand, M., Cazes, A., Monnot, C., . . . Germain, S. (2012). Protection against myocardial infarction and no-reflow through preservation of vascular integrity by angiopoietin-like 4. *Circulation*, 125(1), 140-149. doi:10.1161/CIRCULATIONAHA.111.049072
- Galicia-Garcia, U., Benito-Vicente, A., Jebari, S., Larrea-Sebal, A., Siddiqi, H., Uribe, K. B., . . . Martin, C. (2020). Pathophysiology of Type 2 Diabetes Mellitus. *Int J Mol Sci*, 21(17). doi:10.3390/ijms21176275
- Gamrat, A., Surdacki, M. A., Chyrchel, B., & Surdacki, A. (2020). Endothelial Dysfunction: A Contributor to Adverse Cardiovascular Remodeling and Heart Failure Development in Type 2 Diabetes beyond Accelerated Atherogenesis. *J Clin Med*, 9(7). doi:10.3390/jcm9072090
- Ghosh, A., Gao, L., Thakur, A., Siu, P. M., & Lai, C. W. K. (2017). Role of free fatty acids in endothelial dysfunction. *J Biomed Sci*, 24(1), 50. doi:10.1186/s12929-017-0357-5
- Godo, S., & Shimokawa, H. (2017). Divergent roles of endothelial nitric oxide synthases system in maintaining cardiovascular homeostasis. *Free Radic Biol Med*, 109, 4-10. doi:10.1016/j.freeradbiomed.2016.12.019
- Gschwandtner, M., Derler, R., & Midwood, K. S. (2019). More Than Just Attractive: How CCL2 Influences Myeloid Cell Behavior Beyond Chemotaxis. *Front Immunol*, 10, 2759. doi:10.3389/fimmu.2019.02759
- Habas, K., & Shang, L. (2018). Alterations in intercellular adhesion molecule 1 (ICAM-1) and vascular cell adhesion molecule 1 (VCAM-1) in human endothelial cells. *Tissue Cell*, 54, 139-143. doi:10.1016/j.tice.2018.09.002
- Hamidi, T., Singh, A. K., Veland, N., Vemulapalli, V., Chen, J., Hardikar, S., . . . Chen, T. (2018). Identification of Rpl29 as a major substrate of the lysine methyltransferase Set7/9. *J Biol Chem*, 293(33), 12770-12780. doi:10.1074/jbc.RA118.002890
- Hartge, M. M., Unger, T., & Kintscher, U. (2007). The endothelium and vascular inflammation in diabetes. *Diab Vasc Dis Res*, 4(2), 84-88. doi:10.3132/dvdr.2007.025

- Heintzman, N. D., Stuart, R. K., Hon, G., Fu, Y., Ching, C. W., Hawkins, R. D., . . . Ren, B. (2007). Distinct and predictive chromatin signatures of transcriptional promoters and enhancers in the human genome. *Nat Genet*, *39*(3), 311-318. doi:10.1038/ng1966
- Heo, K. S., Berk, B. C., & Abe, J. (2016). Disturbed Flow-Induced Endothelial Proatherogenic Signaling Via Regulating Post-Translational Modifications and Epigenetic Events. *Antioxid Redox Signal*, *25*(7), 435-450. doi:10.1089/ars.2015.6556
- Holmes, D. (2017). Immunometabolism: Physiologic role of IL-1beta in glucose homeostasis. *Nat Rev Endocrinol*, *13*(3), 128. doi:10.1038/nrendo.2017.11
- Horiuchi, T., Mitoma, H., Harashima, S., Tsukamoto, H., & Shimoda, T. (2010). Transmembrane TNF-alpha: structure, function and interaction with anti-TNF agents. *Rheumatology (Oxford)*, *49*(7), 1215-1228. doi:10.1093/rheumatology/keq031
- Hornbeck, P. V., Kornhauser, J. M., Tkachev, S., Zhang, B., Skrzypek, E., Murray, B., . . . Sullivan, M. (2012). PhosphoSitePlus: a comprehensive resource for investigating the structure and function of experimentally determined post-translational modifications in man and mouse. *Nucleic Acids Res*, *40*(Database issue), D261-270. doi:10.1093/nar/gkr1122
- Huang, R. L., Teo, Z., Chong, H. C., Zhu, P., Tan, M. J., Tan, C. K., . . . Tan, N. S. (2011). ANGPTL4 modulates vascular junction integrity by integrin signaling and disruption of intercellular VE-cadherin and claudin-5 clusters. *Blood*, *118*(14), 3990-4002. doi:10.1182/blood-2011-01-328716
- Hyun, K., Jeon, J., Park, K., & Kim, J. (2017). Writing, erasing and reading histone lysine methylations. *Exp Mol Med*, *49*(4), e324. doi:10.1038/emm.2017.11
- Jenuwein, T. (2006). The epigenetic magic of histone lysine methylation. *FEBS J*, *273*(14), 3121-3135. doi:10.1111/j.1742-4658.2006.05343.x
- Kawashima, S., & Yokoyama, M. (2004). Dysfunction of endothelial nitric oxide synthase and atherosclerosis. *Arterioscler Thromb Vasc Biol*, *24*(6), 998-1005. doi:10.1161/01.ATV.0000125114.88079.96
- Keating, S. T., & El-Osta, A. (2013). Transcriptional regulation by the Set7 lysine methyltransferase. *Epigenetics*, *8*(4), 361-372. doi:10.4161/epi.24234
- Keating, S. T., Ziemann, M., Okabe, J., Khan, A. W., Balcerczyk, A., & El-Osta, A. (2014). Deep sequencing reveals novel Set7 networks. *Cell Mol Life Sci*, *71*(22), 4471-4486. doi:10.1007/s00018-014-1651-y
- Kleinbongard, P., Heusch, G., & Schulz, R. (2010). TNFalpha in atherosclerosis, myocardial ischemia/reperfusion and heart failure. *Pharmacol Ther*, *127*(3), 295-314. doi:10.1016/j.pharmthera.2010.05.002
- Kobayashi, J., & Mabuchi, H. (2015). Lipoprotein lipase and atherosclerosis. *Ann Clin Biochem*, *52*(Pt 6), 632-637. doi:10.1177/0004563215590451
- Kolluru, G. K., Bir, S. C., & Kevil, C. G. (2012). Endothelial dysfunction and diabetes: effects on angiogenesis, vascular remodeling, and wound healing. *Int J Vasc Med*, *2012*, 918267. doi:10.1155/2012/918267
- Kouzarides, T. (2002). Histone methylation in transcriptional control. *Curr Opin Genet Dev*, *12*(2), 198-209. doi:10.1016/s0959-437x(02)00287-3
- Lehnertz, B., Rogalski, J. C., Schulze, F. M., Yi, L., Lin, S., Kast, J., & Rossi, F. M. (2011). p53-dependent transcription and tumor suppression are not affected in

- Set7/9-deficient mice. *Mol Cell*, 43(4), 673-680.
doi:10.1016/j.molcel.2011.08.006
- Li, Y., Reddy, M. A., Miao, F., Shanmugam, N., Yee, J. K., Hawkins, D., . . . Natarajan, R. (2008). Role of the histone H3 lysine 4 methyltransferase, SET7/9, in the regulation of NF-kappaB-dependent inflammatory genes. Relevance to diabetes and inflammation. *J Biol Chem*, 283(39), 26771-26781.
doi:10.1074/jbc.M802800200
- Liu, Z., Lerman, L. O., Tang, H., Barber, C., Wan, L., Hui, M. M., . . . Woolfenden, J. M. (2014). Inflammation imaging of atherosclerosis in Apo-E-deficient mice using a (99m)Tc-labeled dual-domain cytokine ligand. *Nucl Med Biol*, 41(10), 785-792. doi:10.1016/j.nucmedbio.2014.08.004
- Mudau, M., Genis, A., Lochner, A., & Strijdom, H. (2012). Endothelial dysfunction: the early predictor of atherosclerosis. *Cardiovasc J Afr*, 23(4), 222-231.
doi:10.5830/CVJA-2011-068
- Noels, H., Weber, C., & Koenen, R. R. (2019). Chemokines as Therapeutic Targets in Cardiovascular Disease. *Arterioscler Thromb Vasc Biol*, 39(4), 583-592.
doi:10.1161/ATVBAHA.118.312037
- Noma, K., Allis, C. D., & Grewal, S. I. (2001). Transitions in distinct histone H3 methylation patterns at the heterochromatin domain boundaries. *Science*, 293(5532), 1150-1155. doi:10.1126/science.1064150
- Oemar, B. S., Tschudi, M. R., Godoy, N., Brovkovich, V., Malinski, T., & Luscher, T. F. (1998). Reduced endothelial nitric oxide synthase expression and production in human atherosclerosis. *Circulation*, 97(25), 2494-2498.
doi:10.1161/01.cir.97.25.2494
- Ohashi, M., Runge, M. S., Faraci, F. M., & Heistad, D. D. (2006). MnSOD deficiency increases endothelial dysfunction in ApoE-deficient mice. *Arterioscler Thromb Vasc Biol*, 26(10), 2331-2336. doi:10.1161/01.ATV.0000238347.77590.c9
- Okabe, J., Fernandez, A. Z., Ziemann, M., Keating, S. T., Balcerczyk, A., & El-Osta, A. (2014). Endothelial transcriptome in response to pharmacological methyltransferase inhibition. *ChemMedChem*, 9(8), 1755-1762.
doi:10.1002/cmdc.201402091
- Okabe, J., Orłowski, C., Balcerczyk, A., Tikellis, C., Thomas, M. C., Cooper, M. E., & El-Osta, A. (2012). Distinguishing hyperglycemic changes by Set7 in vascular endothelial cells. *Circ Res*, 110(8), 1067-1076.
doi:10.1161/CIRCRESAHA.112.266171
- Olson, F. J., Schmidt, C., Gummesson, A., Sigurdardottir, V., Hulthe, J., Wiklund, O., & Fagerberg, B. (2008). Circulating matrix metalloproteinase 9 levels in relation to sampling methods, femoral and carotid atherosclerosis. *J Intern Med*, 263(6), 626-635. doi:10.1111/j.1365-2796.2008.01927.x
- Paneni, F., Costantino, S., Battista, R., Castello, L., Capretti, G., Chiandotto, S., . . . Cosentino, F. (2015). Adverse epigenetic signatures by histone methyltransferase Set7 contribute to vascular dysfunction in patients with type 2 diabetes mellitus. *Circ Cardiovasc Genet*, 8(1), 150-158.
doi:10.1161/CIRCGENETICS.114.000671
- Peiro, C., Lorenzo, O., Carraro, R., & Sanchez-Ferrer, C. F. (2017). IL-1beta Inhibition in Cardiovascular Complications Associated to Diabetes Mellitus. *Front Pharmacol*, 8, 363. doi:10.3389/fphar.2017.00363

- Petrie, J. R., Guzik, T. J., & Touyz, R. M. (2018). Diabetes, Hypertension, and Cardiovascular Disease: Clinical Insights and Vascular Mechanisms. *Can J Cardiol*, *34*(5), 575-584. doi:10.1016/j.cjca.2017.12.005
- Pober, J. S., & Sessa, W. C. (2007). Evolving functions of endothelial cells in inflammation. *Nat Rev Immunol*, *7*(10), 803-815. doi:10.1038/nri2171
- Rea, S., Eisenhaber, F., O'Carroll, D., Strahl, B. D., Sun, Z. W., Schmid, M., . . . Jenuwein, T. (2000). Regulation of chromatin structure by site-specific histone H3 methyltransferases. *Nature*, *406*(6796), 593-599. doi:10.1038/35020506
- Rosen, E. D., Kaestner, K. H., Natarajan, R., Patti, M. E., Sallari, R., Sander, M., & Susztak, K. (2018). Epigenetics and Epigenomics: Implications for Diabetes and Obesity. *Diabetes*, *67*(10), 1923-1931. doi:10.2337/db18-0537
- Santos-Rosa, H., Schneider, R., Bannister, A. J., Sherriff, J., Bernstein, B. E., Emre, N. C., . . . Kouzarides, T. (2002). Active genes are tri-methylated at K4 of histone H3. *Nature*, *419*(6905), 407-411. doi:10.1038/nature01080
- Sasaki, K., Doi, S., Nakashima, A., Irifuku, T., Yamada, K., Kokoroishi, K., . . . Masaki, T. (2016). Inhibition of SET Domain-Containing Lysine Methyltransferase 7/9 Ameliorates Renal Fibrosis. *J Am Soc Nephrol*, *27*(1), 203-215. doi:10.1681/ASN.2014090850
- Schulz, E., Gori, T., & Munzel, T. (2011). Oxidative stress and endothelial dysfunction in hypertension. *Hypertens Res*, *34*(6), 665-673. doi:10.1038/hr.2011.39
- Sena, C. M., Pereira, A. M., & Seica, R. (2013). Endothelial dysfunction - a major mediator of diabetic vascular disease. *Biochim Biophys Acta*, *1832*(12), 2216-2231. doi:10.1016/j.bbadis.2013.08.006
- Shi, Y., Lan, F., Matson, C., Mulligan, P., Whetstone, J. R., Cole, P. A., . . . Shi, Y. (2004). Histone demethylation mediated by the nuclear amine oxidase homolog LSD1. *Cell*, *119*(7), 941-953. doi:10.1016/j.cell.2004.12.012
- Sims, R. J., 3rd, Nishioka, K., & Reinberg, D. (2003). Histone lysine methylation: a signature for chromatin function. *Trends Genet*, *19*(11), 629-639. doi:10.1016/j.tig.2003.09.007
- Stelzer, G., Rosen, N., Plaschkes, I., Zimmerman, S., Twik, M., Fishilevich, S., . . . Lancet, D. (2016). The GeneCards Suite: From Gene Data Mining to Disease Genome Sequence Analyses. *Curr Protoc Bioinformatics*, *54*, 1 30 31-31 30 33. doi:10.1002/cpbi.5
- Steyers, C. M., 3rd, & Miller, F. J., Jr. (2014). Endothelial dysfunction in chronic inflammatory diseases. *Int J Mol Sci*, *15*(7), 11324-11349. doi:10.3390/ijms150711324
- Strahl, B. D., & Allis, C. D. (2000). The language of covalent histone modifications. *Nature*, *403*(6765), 41-45. doi:10.1038/47412
- Subramanian, K., Jia, D., Kapoor-Vazirani, P., Powell, D. R., Collins, R. E., Sharma, D., . . . Vertino, P. M. (2008). Regulation of estrogen receptor alpha by the SET7 lysine methyltransferase. *Mol Cell*, *30*(3), 336-347. doi:10.1016/j.molcel.2008.03.022
- Szicsz, E., Pap, D., Lippai, R., Beres, N. J., Fekete, A., Szabo, A. J., & Vannay, A. (2015). Fibrosis Related Inflammatory Mediators: Role of the IL-10 Cytokine Family. *Mediators Inflamm*, *2015*, 764641. doi:10.1155/2015/764641
- Takeda, Y., Matoba, K., Sekiguchi, K., Nagai, Y., Yokota, T., Utsunomiya, K., & Nishimura, R. (2020). Endothelial Dysfunction in Diabetes. *Biomedicines*, *8*(7). doi:10.3390/biomedicines8070182

- Takemoto, Y., Ito, A., Niwa, H., Okamura, M., Fujiwara, T., Hirano, T., . . . Yoshida, M. (2016). Identification of Cyproheptadine as an Inhibitor of SET Domain Containing Lysine Methyltransferase 7/9 (Set7/9) That Regulates Estrogen-Dependent Transcription. *J Med Chem*, 59(8), 3650-3660. doi:10.1021/acs.jmedchem.5b01732
- Tamaru, H., Zhang, X., McMillen, D., Singh, P. B., Nakayama, J., Grewal, S. I., . . . Selker, E. U. (2003). Trimethylated lysine 9 of histone H3 is a mark for DNA methylation in *Neurospora crassa*. *Nat Genet*, 34(1), 75-79. doi:10.1038/ng1143
- Tseng, W. L., Chou, S. J., Chiang, H. C., Wang, M. L., Chien, C. S., Chen, K. H., . . . Yu, W. C. (2017). Imbalanced Production of Reactive Oxygen Species and Mitochondrial Antioxidant SOD2 in Fabry Disease-Specific Human Induced Pluripotent Stem Cell-Differentiated Vascular Endothelial Cells. *Cell Transplant*, 26(3), 513-527. doi:10.3727/096368916X694265
- van den Oever, I. A., Raterman, H. G., Nurmohamed, M. T., & Simsek, S. (2010). Endothelial dysfunction, inflammation, and apoptosis in diabetes mellitus. *Mediators Inflamm*, 2010, 792393. doi:10.1155/2010/792393
- Veerappan, C. S., Avramova, Z., & Moriyama, E. N. (2008). Evolution of SET-domain protein families in the unicellular and multicellular Ascomycota fungi. *BMC Evol Biol*, 8, 190. doi:10.1186/1471-2148-8-190
- Wilson, J. R., Jing, C., Walker, P. A., Martin, S. R., Howell, S. A., Blackburn, G. M., . . . Xiao, B. (2002). Crystal structure and functional analysis of the histone methyltransferase SET7/9. *Cell*, 111(1), 105-115. doi:10.1016/s0092-8674(02)00964-9
- Xiao, B., Jing, C., Wilson, J. R., Walker, P. A., Vasisht, N., Kelly, G., . . . Gamblin, S. J. (2003). Structure and catalytic mechanism of the human histone methyltransferase SET7/9. *Nature*, 421(6923), 652-656. doi:10.1038/nature01378
- Xu, L., Guo, Z. N., Yang, Y., Xu, J., Burchell, S. R., Tang, J., . . . Zhang, J. H. (2015). Angiopoietin-like 4: A double-edged sword in atherosclerosis and ischemic stroke? *Exp Neurol*, 272, 61-66. doi:10.1016/j.expneurol.2015.05.020
- Yang, J., Li, X., & Xu, D. (2021). Research Progress on the Involvement of ANGPTL4 and Loss-of-Function Variants in Lipid Metabolism and Coronary Heart Disease: Is the "Prime Time" of ANGPTL4-Targeted Therapy for Coronary Heart Disease Approaching? *Cardiovasc Drugs Ther*, 35(3), 467-477. doi:10.1007/s10557-020-07001-0
- Yang, J. X., Pan, Y. Y., Ge, J. H., Chen, B., Mao, W., Qiu, Y. G., & Wang, X. X. (2016). Tanshinone II A Attenuates TNF-alpha-Induced Expression of VCAM-1 and ICAM-1 in Endothelial Progenitor Cells by Blocking Activation of NF-kappaB. *Cell Physiol Biochem*, 40(1-2), 195-206. doi:10.1159/000452537
- Yu, C., & Zhuang, S. (2019). Histone Methyltransferases as Therapeutic Targets for Kidney Diseases. *Front Pharmacol*, 10, 1393. doi:10.3389/fphar.2019.01393
- Zhang, X., Huang, Y., & Shi, X. (2015). Emerging roles of lysine methylation on non-histone proteins. *Cell Mol Life Sci*, 72(22), 4257-4272. doi:10.1007/s00018-015-2001-4
- Zhang, Y., & Reinberg, D. (2001). Transcription regulation by histone methylation: interplay between different covalent modifications of the core histone tails. *Genes Dev*, 15(18), 2343-2360. doi:10.1101/gad.927301

- Zheng, Q., Prescott, N. A., Maksimovic, I., & David, Y. (2019). (De)Toxifying the Epigenetic Code. *Chem Res Toxicol*, 32(5), 796-807.
doi:10.1021/acs.chemrestox.9b00013
- Zheng, Y., Ley, S. H., & Hu, F. B. (2018). Global aetiology and epidemiology of type 2 diabetes mellitus and its complications. *Nat Rev Endocrinol*, 14(2), 88-98.
doi:10.1038/nrendo.2017.151